Scientific Reports

https://doi.org/10.1038/s41598-026-50820-8

Article in Press

Effects of adjuvant propofol on antitumoral effects of carboplatin in experimental endometrial cancer: possible epigenetic associations

Received: 27 February 2026

Accepted: 23 April 2026

Published online: 21 May 2026

Cite this article as: Gürel Ç., Kuşçu G.C., Buhur A. *et al.* Effects of adjuvant propofol on antitumoral effects of carboplatin in experimental endometrial cancer: possible epigenetic associations. *Sci Rep* (2026). https://doi.org/10.1038/s41598-026-50820-8

Çevik Gürel, Gökçe Ceren Kuşçu, Aylin Buhur, Saadet Özen Akarca Dizakar, Hale Güler Kara, Neslihan Pınar Özateş, Nuri Yıldırım & İlkben Günüşen

Effects of Adjuvant Propofol on Antitumoral Effects of Carboplatin in Experimental Endometrial Cancer: Possible Epigenetic Associations

Çevik Gürel[1,*], Gökçe Ceren Kuşçu[2], Aylin Buhur[3], Saadet Özen Akarca Dizakar[4], Hale Güler Kara[5], Neslihan Pınar Özateş[5], Nuri Yıldırım[6], İlkben Günüşen[7]

[1] Department of Histology and Embryology, Faculty of Medicine, Harran University, Şanlıurfa, Türkiye

[2] Department of Histology and Embryology, Faculty of Medicine, Ege University, İzmir, Türkiye

[3] Department of Basic Sciences, Faculty of Dentistry, İstanbul Galata University, İstanbul, Türkiye

[4] Department of Histology and Embryology, Faculty of Medicine, Bakırçay University, Izmir, Türkiye

[5] Department of Medical Biology, Faculty of Medicine, Harran University, Şanlıurfa, Türkiye

[6] Department of Obstetrics and Gynecology, Faculty of Medicine, Ege University, İzmir, Türkiye

[7] Department of Anesthesiology and Reanimation, Faculty of Medicine, Ege University, İzmir, Türkiye

Corresponding Author: Çevik Gürel, PhD

Corresponding Author E-mail: cevikgurel@harran.edu.tr; cevikgurel@gmail.com

ORCIDs

Çevik Gürel 0000-0003-0266-2115

Gökçe Ceren Kuşçu 0000-0003-1750-8209

Aylin Buhur 0000-0002-3759-6616
Saadet Özen Akarca Dizakar 0000-0002-4358-6510
Hale Güler Kara 0000-0002-4304-3727
Neslihan Pınar Özateş 0000-0001-6856-4644
Nuri Yıldırım 0000-0002-0605-4750
İlkben Günüşen 0000-0002-8719-0358

Abstract

Endometrial cancer (EC) is a gynecological malignancy classified into two biologically distinct subtypes, Type I and Type II EC. The more aggressive Type II EC exhibits a poor response to conventional platinum-based chemotherapy. Propofol, an anesthetic agent in gynecologic surgery, has been reported to exert antitumor effects beyond anesthesia; however, its role as a chemoadjuvant in EC remains insufficiently explored. In this study, we investigated the effects of propofol combined with carboplatin on drug resistance- and metastasis-associated microRNAs and genes using *in vitro* and *in vivo* Type II EC model. Propofol treatment significantly reduced cancer cell viability and migratory capacity, while the combination treatment showed greater antimetastatic effects compared with carboplatin alone. In xenograft models, combination therapy resulted in a significant reduction in tumor volume and suggested reduced metastatic involvement in lung and liver tissues. Molecular analyses revealed downregulation of oncogenic microRNAs (miR-21, miR-135a) and upregulation of tumor-suppressive microRNAs (miR-34b, miR-98), accompanied by reduced mTOR, c-Myc, MRP7, and N-cadherin expression and increased PTEN and HMGB1 levels. Collectively, these findings indicate that propofol is associated with greater antitumor effects when combined with carboplatin, accompanied by changes in miRNA-gene expression patterns.

Keywords: Drug Resistance, Endometrial Cancer, Carboplatin, Metastasis, MicroRNA, Propofol

Introduction

Endometrial cancer (EC) is the most common gynecological malignancy in developed countries [1], and it is responsible for more than 2% of cancer-related deaths among women worldwide [2]. Considered a serious global public health problem due to its high incidence and mortality rates, this gynecological malignancy is broadly classified into two subtypes based on etiological and pathophysiological characteristics: Type I and Type II EC. Type I EC constitutes approximately 60–70% of cases and is predominantly composed of low-grade (G1-G2) endometrioid carcinomas, which are associated with hyperestrogenic conditions, atypical endometrial hyperplasia, and Lynch syndrome. In contrast, Type II EC, which includes high-grade (G3) endometrioid, serous, clear cell, and undifferentiated subtypes, is closely associated with endocrine disorders such as diabetes mellitus and polycystic ovary syndrome and is also characterized by chromosomal instability and frequent p53 mutation [3,4].

Compared with Type I EC, Type II EC is associated with a poorer prognosis, and the standard treatment consists of total hysterectomy with bilateral salpingo-oophorectomy and lymphadenectomy [1]. In addition, adjuvant radiotherapy and chemotherapy are commonly employed, particularly in patients with metastasis, as part of a multimodal treatment strategy [1,5]. Despite the clinical benefits provided by these therapeutic approaches, recurrence rates of Type II EC exceed 50% within 2–3 years following surgical intervention [5,6]. As a result, Type II EC contributes disproportionately to EC-related mortality despite representing a

smaller fraction of overall EC cases [7]. This highly aggressive clinical course of Type II EC is largely attributable to its distinct molecular and biological characteristics. Indeed, Type II EC is commonly defined by extensive chromosomal instability and frequent alterations in key oncogenic pathways [8]. Collectively, these molecular abnormalities drive rapid tumor progression, early dissemination, and a pronounced tendency toward chemoresistance, thereby limiting the long-term efficacy of standard platinum-based chemotherapy [9,10].

MicroRNAs (miRNAs) are small non-coding RNA molecules that fine-tune gene expression at the post-transcriptional level through interaction with the 3′ untranslated regions of target messenger RNAs (mRNAs), resulting in mRNA degradation or inhibition of translation [11]. These small regulatory molecules are estimated to regulate approximately 60% of protein-coding genes, with each miRNA targeting an average of 200 transcripts, underscoring their critical regulatory role in diverse physiological and pathological processes, including cancer development and progression [12,13]. In the context of EC, miRNAs have been identified as central modulators of numerous signaling pathways, playing critical roles in tumor initiation, progression, metastatic dissemination, and the development of chemoresistance [14,15]. For example, miR-21 has been found to enhance cell proliferation, invasion, and metastatic potential while suppressing apoptosis in EC through post-transcriptional regulation of its target gene PTEN [16]. Along similar lines, miR-135a [17] and miR-423 [18] have been linked to chemoresistance in EC and to the regulation of cell migration and invasion, through modulation of Akt signaling and N-cadherin expression, respectively. Moreover, miR-let-7c has been documented to suppress Aurora B expression in EC cells, thereby contributing to the development of paclitaxel resistance in these cells [19]. Conversely, accumulating evidence indicates that a subset of miRNAs functions as tumor suppressors in EC through the coordinated control of target genes associated with migration, invasion, metastasis, and chemoresistance. Accordingly, miR-1/133 [20], miR-205, miR-449 [21], and miR-34b [22] have been demonstrated to exert anti-metastatic effects in EC through regulation of PDE7A, mTOR, PTEN, and c-Myc, respectively. In addition, miR-98 [23] and miR-200c [24] have been implicated in enhancing chemosensitivity in EC cells by targeting MRP7 and TUBB3, respectively. In this context, identifying factors that govern miRNA activity and unraveling their mechanistic impact represents a critical step toward the development of effective therapeutic strategies against chemoresistance and metastasis in Type II EC.

Propofol (2,6-diisopropylphenol) is a short-acting intravenous hypnotic alkylphenol derivative that is widely used for anesthesia induction and maintenance, as well as for sedation in clinical practice [25]. In addition to its anesthetic properties, propofol exerts antitumor activity across a broad spectrum of malignancies, directly or indirectly influencing cancer development [26]. Converging experimental evidence demonstrates that propofol suppresses the malignant phenotype of multiple human cancers, including hepatocellular carcinoma, breast cancer, lung cancer, and pancreatic cancer, by modulating miRNAs involved in key signaling pathways such as HIF-1α, MAPK, NF-κB, and Nrf2 [27]. Moreover, accumulating evidence indicates that propofol, when administered as an adjuvant to chemotherapy, reduces chemoresistance and enhances chemotherapy-induced apoptosis across multiple cancer types [28]. For instance, Du et al. demonstrated that propofol decreases the DNA-binding activity of NF-κB in pancreatic cancer cells, thereby increasing their sensitivity to gemcitabine [29]. Similarly, propofol has been shown to support paclitaxel-induced apoptosis in ovarian cancer cells through inhibition of the transcription factor Slug [30], and to increase cisplatin sensitivity in human lung cancer cells [31]. In light of this body of evidence, it can be reasonably suggested that propofol, when administered as an adjuvant to chemotherapeutic agents, may represent a promising approach associated with increased chemotherapy effectiveness. On the other hand, carboplatin, which is used in cancer treatment as a less cytotoxic alternative to cisplatin [32], achieves response rates ranging from 28% to 33% in patients with advanced, recurrent, or metastatic EC [33]. Therefore, clinical and preclinical studies aimed at enhancing carboplatin responsiveness continue to represent a central focus of research efforts directed toward the development of novel therapeutic strategies in EC [33]. However, despite numerous studies reporting that propofol reduces chemoresistance and enhances chemotherapy-induced apoptosis across various cancer types, no studies addressing its use as an adjuvant to carboplatin in Type II EC have been identified in the current literature.

In this context, the present study aimed to investigate whether propofol, when administered in combination with carboplatin, is associated with alterations in chemoresistance- and metastasis-related molecular pathways in Type II EC models, and whether such alterations correspond to changes in tumor cell behavior *in vitro* and *in vivo*.

Material and Methods

Cell Lines and Cell Culture

PTEN-negative AN3CA cells isolated from metastatic lesions in the lymph nodes of a patient with advanced EC produce poorly differentiated and platinum-resistant malignant tumors and more closely reflect the clinical-pathological features of more aggressive EC (Type II) with a higher predisposition to recurrent or metastatic disease [34]. Based on these characteristics, the AN3CA cell line was selected for use in the present study.

AN3CA cell line was obtained from the American Type Culture Collection (HTB-111; ATCC, Manassas, VA, USA). Cells were thawed according to the manufacturer's instructions and seeded into culture flasks (707003; Nest Scientific, Nest, New Jersey, USA) containing minimum essential medium (MEM) (MEM-A; Capricorn Scientific, Ebsdorfergrund, Germany) supplemented with 10% fetal bovine serum (FBS) and 1% penicillin–streptomycin (PS-B; Capricorn Scientific, Ebsdorfergrund, Germany), then incubated at 37 °C in a humidified atmosphere with 5% CO_2.

In the *in vitro* experiments, immortalized human endometrial stromal (HES) cells were used to evaluate the effects of the tested treatment protocol on healthy endometrial cells. The HES cell line was obtained from Applied Biological Materials (T0533; ABM, Richmond, Canada) and thawed according to the manufacturer's instructions. Cells were seeded into Dulbecco's Modified Eagle Medium (DMEM) (DMEM-12-A; Capricorn Scientific, Ebsdorfergrund, Germany) supplemented with 10% fetal bovine serum (FBS) and 1% penicillin–streptomycin (PS-B; Capricorn Scientific, Ebsdorfergrund, Germany), then incubated at 37 °C in a humidified atmosphere with 5% CO_2.

Cells cultured as described above had their growth medium replaced every two days. Upon reaching approximately 80% confluence, cells were detached using 0.25% trypsin–EDTA (TRY-3B; Capricorn Scientific, Ebsdorfergrund, Germany, resuspended, and reseeded. Cells passaged three times under these conditions were subsequently used for *in vitro* experiments.

Drug Preparation

Propofol and carboplatin were prepared according to the manufacturers' instructions. Briefly, both compounds were initially dissolved in dimethyl sulfoxide (DMSO) (sc-358801; Santa Cruz, Texas, USA) to generate stock

solutions and subsequently diluted in culture medium to achieve the desired final working concentrations.

The final working concentrations of propofol [5] and carboplatin [34] were determined based on previously published studies.

The final DMSO concentration was kept below 0.1% in all treatment conditions, as concentrations at or below this level are generally considered non-cytotoxic [35].

In Vitro Experiment Design

After cell culture and passaging, the following *in vitro* experimental groups were established:

HES+DMSO: Cells in this group were treated with vehicle only and incubated in DMEM supplemented with 10% FBS and 1% penicillin–streptomycin, DMSO at the same final concentration used in the drug-treated groups, for 24, 48, and 72 h. This group served as the vehicle control in all subsequent analyses. Following incubation, cells were subjected to viability, proliferation, migration, and molecular assays.

HES+Propofol: Cells were treated with propofol (HY-B0649-100mg; MedChemExpress, New Jersey, USA) at a final working concentration of 4 µg/mL [5] in complete culture medium, with a total volume of 100 µL per well. Propofol stock solutions were prepared in DMSO and diluted into culture medium to achieve the desired final concentration. Cells were incubated for 24, 48, and 72 h. The final DMSO concentration was kept constant across all experimental groups. Following incubation, cells were subjected to viability, proliferation, migration, and molecular assays.

HES+Carboplatin: Cells in this group were treated with carboplatin (HY-17393-500mg; MedChemExpress, New Jersey, USA) at a final working concentration of 125 µg/m [34] in complete culture medium, with a total volume of 100 µL per well. Carboplatin stock solutions were prepared in DMSO and diluted into culture medium to achieve the desired final concentration. Cells were incubated for 24, 48, and 72 h. The final DMSO concentration was kept constant across all experimental groups. Following incubation, cells were subjected to viability, proliferation, migration, and molecular assays.

HES+Propofol-Carboplatin: Cells in this group were treated with a combination of carboplatin (125 µg/mL) and propofol (4 µg/mL) in complete

culture medium, with a total volume of 100 µL per well. Cells were incubated for 24, 48, and 72 h. The final DMSO concentration was kept constant across all experimental groups. Following incubation, cells were subjected to viability, proliferation, migration, and molecular assays.

AN3CA+DMSO: Cells were incubated for 24, 48, and 72 h in MEM supplemented with 10% FBS and 1% penicillin–streptomycin, containing, DMSO at the same final concentration used in the treatment groups, and served as the vehicle control in subsequent analyses. Following incubation, cells were subjected to viability, proliferation, migration, and molecular assays.

AN3CA+Propofol: Cells were treated with propofol at a final working concentration of 4 µg/mL [5] in complete culture medium, with a total volume of 100 µL per well. Propofol stock solutions were prepared in DMSO and diluted into culture medium to achieve the desired final concentration. Cells were incubated for 24, 48, and 72 h. The final DMSO concentration was kept constant across all experimental groups. Following incubation, cells were subjected to viability, proliferation, migration, and molecular assays.

AN3CA+Carboplatin: Cells in this group were treated with carboplatin at a final working concentration of 125 µg/m [34] in complete culture medium, with a total volume of 100 µL per well. Carboplatin stock solutions were prepared in DMSO and diluted into culture medium to achieve the desired final concentration. Cells were incubated for 24, 48, and 72 h. The final DMSO concentration was kept constant across all experimental groups. Following incubation, cells were subjected to viability, proliferation, migration, and molecular assays.

AN3CA+Propofol-Carboplatin: Cells in this group were treated with a combination of carboplatin (125 µg/mL) and propofol (4 µg/mL) in complete culture medium, with a total volume of 100 µL per well. Cells were incubated for 24, 48, and 72 h. The final DMSO concentration was kept constant across all experimental groups. Following incubation, cells were subjected to viability, proliferation, migration, and molecular assays.

3-(4,5-dimethylthiazol-2-yl)-2,5-diphenyltetrazolium bromide (MTT) assay

The MTT assay was performed according to the manufacturer's instructions using a commercially available kit (E-CK-A341; Elabscience®, Texas, USA). Briefly, AN3CA and HES cells were seeded into 96-well plates at a density of 2×10^3 cells per well in 100 µL of culture medium. After 24 h of incubation, experimental

treatments were applied, and at 24, 48, and 72 h, 1× MTT working solution was added to each well. Cells were incubated for an additional 4 h, after which absorbance was measured at 570 nm using a microplate reader. The resulting optical density values were recorded for subsequent analysis.

Wound Healing Assay

The wound healing assay was performed to evaluate the migratory capacity of cancer cells, as previously described by Fan et al. [36]. Briefly, cells treated with DMSO, propofol, carboplatin, or carboplatin + propofol were detached using trypsin, resuspended in MEM or DMEM, and seeded into 6-well plates at a density of 1×10^5 cells per well. Cells were incubated in MEM or DMEM supplemented with 10% FBS at 37 °C in a humidified atmosphere containing 5% CO_2 until approximately 75% confluence was reached. A linear wound was generated across the center of the cell monolayer using a 100 µl sterile pipette tip, and floating cells were removed by washing three times with 1× PBS. To limit the contribution of cell proliferation to wound closure, cells were maintained in medium containing reduced serum levels (1% FBS) following scratch generation under the same conditions, and images were captured at 0 and 48 h. Migration inhibition (%) was calculated using the formula [(wound width at 0 h − wound width at 48 h) / wound width at 0 h] × 100, with wound areas quantified using ImageJ software [37].

Transwell Invasion Assay

The transwell invasion assay performed to evaluate the invasive capacities of cells, following the protocol described by Fan et al. [36]. Briefly, polycarbonate membrane inserts with an 8.0-µm pore size compatible with 24-well plates (725301; Nest Scientific, Phoenix, USA) were coated with Matrigel diluted 1:8 in MEM or DMEM prior to the assay. Cells previously treated with DMSO, propofol, carboplatin, or carboplatin plus propofol were trypsinized, resuspended, and seeded into the upper chambers at a density of 1×10^5 cells per well in 100 µL of serum-free MEM/DMEM, while 600 µL of medium was added to the lower chambers as a chemoattractant. The plates were incubated for 24 h at 37°C in a humidified atmosphere containing 5% CO_2. Following incubation, non-invading cells on the upper surface of the membrane were gently removed, whereas cells that had invaded to the lower surface were fixed with 4% paraformaldehyde for 30 min and stained with crystal violet. Invaded cells were then visualized and photographed using a light microscope (BX5; Olympus, Tokyo, Japan).

Measurement of Caspase-3 Activity

Caspase-3 enzymatic activity was quantified using a fluorometric assay kit (5723; Cell Signaling Technology, Danvers, MA, USA) according to the manufacturer's instructions. Following the washing steps, fluorescence intensity was measured using a microplate reader at an excitation wavelength of 380 nm and an emission wavelength of 450 nm. Caspase-3 activity was calculated from the fluorescence signal and expressed as fold change relative to the control group [38].

Immunofluorescence (IF) Staining and Analysis

HES and AN3CA cells were fixed in 4% paraformaldehyde (PFA) (158127; Sigma, Darmstadt, Germany) for 15 min, permeabilized with 0.1% Triton X-100 for 10 min at room temperature, and blocked with 5% bovine serum albumin for 1 h. Cells were then incubated overnight at 4°C with primary antibodies (Table 1) diluted at the optimal concentration, followed by incubation with FITC-conjugated secondary antibodies for 1 h at room temperature. Nuclei were counterstained with DAPI. Fluorescence signals were visualized using a fluorescence microscope (BX51; Olympus, Tokyo, Japan). Mean intracellular fluorescence intensity was quantified using ImageJ (version 1.46; NIH, Maryland, USA) software. Three representative images were acquired per group, and at least 30 cells were analyzed for each condition.

Animals and Ethical Statement

All experimental procedures were performed in compliance with the guidelines outlined in the Guide for the Care and Use of Laboratory Animals published by the National Institutes of Health. The experimental protocol was reviewed and approved by Ege University Animal Experimentation Local Ethics Committee (Approval Number: 2023-019; Approval Date: March 29, 2023).

Following the approval of the relevant ethical committees, a total of 50 female nude CD1 mice aged 4–5 weeks were used for the *in vivo* phase of the study. The animals were obtained from Kobay A.Ş. (Kobay A.Ş., Ankara, Türkiye)

In Vivo Experimental Design

After a one-week acclimatization period, 10 randomly selected mice were assigned to the Control group. In the remaining 40 animals, a Type II EC model was established by subcutaneous injection of AN3CA cells that had been cultured under sterile conditions and passaged three times at the Molecular Embryology Laboratory of the Department of Histology and Embryology, Ege University Faculty of Medicine.

The Type II EC xenograft model was established according to previously published protocols [39–41]. Briefly, AN3CA cells cultured under sterile conditions and passaged three times were resuspended in 1× phosphate buffered saline (PBS) (P4417; Sigma, Darmstadt, Germany) at a concentration of 5×10^6 cells per 100 µL. Subsequently, 100 µL of the cell suspension was subcutaneously injected into the right hind flank of each mouse to generate the xenograft tumors. Mice were monitored for one week following inoculation, after which tumor dimensions were measured every four days using a digital caliper. Tumor volume was calculated using the formula (length × width^2)/2 mm^3. When tumor volume reached ≥100 mm^3, animals were randomly allocated into four groups (n = 10 per group). The day of group allocation was defined as day 0, and all experimental procedures were performed accordingly.

The experimental groups established for *in vivo* studies and the corresponding experimental procedures applied to each group are described below:

Control group (n = 10): Animals in this group were left untreated, with no experimental manipulation or pharmacological intervention, and served as the negative control.

Type II EC+Saline group (n = 10): Animals bearing the Type II EC xenograft received intraperitoneal (i.p.) injections of 200 µL sterile saline on experimental days 14, 21, 28, and 35 at 7-day intervals [34]. Tumor volume and body weight were recorded on days 0, 7, 14, 21, 28, 35, and 42. Animals were euthanized at the end of the experiment on day 42 [39,41].

Type II EC + Propofol group (n = 10): Animals received propofol at a dose of 50 mg/kg via i.p. injection on days 14, 21, 28, and 35 [34,42]. Propofol was initially dissolved in DMSO and further diluted in sterile saline prior to administration; the final DMSO concentration was kept below 0.1% in all treatment conditions, as concentrations at or below this level are generally considered non-cytotoxic [35]. In this group, propofol was administered as a single bolus injection. Tumor volume and body weight were monitored at the indicated time points, and animals were sacrificed on day 42.

Type II EC + Carboplatin group (n = 10): Animals in this group were treated with carboplatin (50 mg/kg, i.p.) on days 14, 21, 28, and 35 [34,42]. Carboplatin was initially dissolved in DMSO and further diluted in sterile saline prior to administration; the final DMSO concentration was kept below 0.1% in all treatment conditions, as concentrations at or below this level are generally

considered non-cytotoxic [35]. In this group, carboplatin was administered as a single bolus injection. Tumor growth and body weight were measured at regular intervals from day 0 to day 42, after which animals were euthanized.

Type II EC + Carboplatin + Propofol group (n = 10): Animals received carboplatin (50 mg/kg, i.p.), followed 30 minutes later by propofol (50 mg/kg, i.p.), on days 14, 21, 28, and 35 [42]. Carboplatin and propofol were initially dissolved in DMSO and further diluted in sterile saline prior to administration; the final DMSO concentration was kept below 0.1% in all treatment conditions, as concentrations at or below this level are generally considered non-cytotoxic [35]. In this group, drugs were administered as a single bolus injection. Tumor volume and body weight were assessed periodically throughout the study, and animals were sacrificed on day 42.

Throughout the experimental period, animals were housed at the Ege University ARGEFAR Preclinical Research Unit in sawdust-bedded cages in groups of five and were provided with a standard laboratory diet, with food and water available ad libitum. The room temperature was maintained at 24 ± 1 °C under a 12-h light/dark cycle, and experiments were conducted in a controlled environment with daily cage cleaning.

At the end of the study, all animals were deeply anesthetized with a single intraperitoneal dose of ketamine (80 mg/kg; Ketalar, Pfizer, Istanbul, Türkiye) and xylazine (10 mg/kg; Rompun, Bayer, Istanbul, Türkiye). Adequate anesthetic depth was confirmed by the absence of pedal withdrawal and corneal reflexes. Euthanasia was then performed by cervical dislocation, and death was verified prior to tissue collection. Tumor tissues were promptly excised along with adjacent normal tissue. In addition, samples from the liver, lungs, brain, and spleen were collected to evaluate metastatic dissemination.

Real-Time Quantitative PCR Analysis

Tissue and cell samples were lysed in 1 mL of TriPure Isolation Reagent containing guanidinium thiocyanate (Roche) and homogenized using a glass–Teflon homogenizer. Total RNA was extracted in accordance with the manufacturer’s protocol. RNA concentration and purity were determined by spectrophotometric analysis. Complementary DNA (cDNA) was synthesized from 1 µg of total RNA using the Transcriptor First Strand cDNA Synthesis Kit (Roche), following the supplier’s instructions.

Quantitative real-time PCR was carried out using SYBR® Green PCR Master Mix (Thermo Fisher Scientific) on a LightCycler 480 Real-Time PCR System (Roche). GAPDH served as the internal reference gene, and all samples were analyzed in triplicate. Relative gene expression levels were calculated using the comparative $2^{-(\Delta\Delta Ct)}$ method. The same procedure was applied to the cells at 24, 48, and 72 hours.

Primer sequences employed in the analyses are provided in Table 2.

Tissue Processing and Histological Staining

Tissue specimens collected for histological evaluation were fixed in 4% PFA (158127; Sigma, Darmstadt, Germany) for 48 h, followed by dehydration through a graded series of ethanol solutions and clearing in xylene. Subsequently, the samples were embedded in paraffin, and 5-µm-thick transverse sections were prepared. Prior to histological analyses, the sections were deparaffinized using xylene.

To evaluate general cytoarchitecture, sections were deparaffinized, rehydrated, and stained with hematoxylin for 3 min. Following differentiation in acid alcohol and bluing in ammoniated water, eosin staining was applied for 1 min. Sections were dehydrated, cleared, and mounted using Entellan (1.07960; Sigma, Darmstadt, Germany).

Histopathological Evaluation for Metastasis

Histopathological assessments were performed independently by four experienced investigators (two histologists and two clinicians), all of whom were blinded to the experimental groups. For each animal, two sections were randomly selected and evaluated. Lung, liver, spleen, and brain sections were examined for the presence and number of metastatic foci. The number of metastatic foci was manually counted under light microscopy, and the final values were calculated as the mean of all observers. This approach was used to minimize observer bias and variability.

Immunohistochemical Analysis, Image Acquisition and Quantitative Analysis

Endogenous peroxidase activity was quenched by incubating the sections in 10% hydrogen peroxide (H1009; Sigma, Darmstadt, Germany) for 30 min. Non-specific binding was subsequently reduced by a 1-h incubation in blocking solution (SHP125; Scytec, Utah, USA) at room temperature. The sections were then

exposed to the appropriate primary antibodies (Table 1) overnight at 4 °C. Following washing steps, sections were sequentially incubated with biotin-conjugated secondary antibodies and horseradish peroxidase (HRP)–linked streptavidin (SHP125; Scytec, Utah, USA). Signal detection was achieved using 3,3′-diaminobenzidine (DAB; ACK125, Scytec, Utah, USA), and nuclei were counterstained with Mayer's hematoxylin (MHS32; Sigma, Darmstadt, Germany).

Bright-field images were captured using a light microscope (BX5; Olympus, Tokyo, Japan). For each animal, three randomly selected coronal sections were evaluated, and ten non-overlapping fields per section were analyzed. Quantitative assessment of immunoreactivity was performed using ImageJ software. Stained regions were identified by color thresholding, and immunopositive signals were calculated as a proportion of the total tissue area after normalization of integrated density values [43].

Statistical Analysis

Statistical evaluations were carried out using GraphPad Prism version 5 (GraphPad Software, La Jolla, CA, USA). After all experimental procedures were finalized, differences among groups were analyzed by one-way ANOVA, and Tukey's multiple comparison test was applied for post hoc analyses. For experiments involving multiple variables (e.g., time and treatment), two-way ANOVA was applied where appropriate. Results are expressed as mean values with corresponding standard errors. Statistical significance thresholds were defined as $p < 0.05$, $p < 0.001$, and $p < 0.0001$.

Results

Adjuvant Propofol is Associated with Greater Carboplatin-Mediated Suppression of Tumor Growth and Migration

In vitro, MTT assays revealed that propofol did not significantly affect the proliferation of HES cells; however, a slight numerical difference was observed compared with the DMSO control that did not reach statistical significance, whereas carboplatin significantly reduced HES cell viability at all time points ($p<0.05$). This cytotoxic effect was partially attenuated in the combination treatment group (Figure 1A).

In contrast, propofol significantly decreased AN3CA cell viability at 24, 48, and 72 h ($p<0.05$), with findings at 72 h being consistent with increased apoptotic activity (Figure 1A). Notably, adjuvant propofol administration further increased

the antiproliferative and apoptotic effects of carboplatin, reducing AN3CA cell viability to approximately 20% at 72 h ($p<0.05$).

Consistently, wound healing (Figure 1C–D), Caspase-3 activity (Figure 1E), and transwell migration assays (Figure 1F) demonstrated that propofol significantly reduced AN3CA cell migration and increased apoptotic activity, while carboplatin exerted a stronger inhibitory effect that was further increased in the combination treatment compared with either treatment alone ($p<0.05$).

>Figure 1<

In vivo, untreated Type II EC xenografts exhibited progressive tumor growth (Figure 2A), whereas significant tumor regression was observed from day 21 onward in Propofol-, Carboplatin-, and combination-treated groups (Figure 2B), with the greatest reduction in tumor volume observed in the combined Propofol–Carboplatin group ($p<0.05$).

>Figure 2<

Collectively, these data suggest that propofol is associated with increased carboplatin-mediated suppression of tumor growth and migration in this experimental model, while showing relatively limited effects in HES cells.

Adjuvant Propofol is Possibly Associated with Carboplatin-Mediated Reprogramming of Metastasis- and Drug Resistance–Related Gene and miRNA Expression

RT-qPCR analyses performed at 24, 48, and 72 h demonstrated that propofol treatment, either alone or in combination with carboplatin, was associated with reduced expression of genes linked to metastasis, drug resistance, and angiogenesis, including mTOR, c-Myc, N-Cadherin, and MRP7, in EC cells. In contrast, the expression of tumor suppressor genes with established antitumoral activity, such as HMGB1 and PTEN, was significantly upregulated across all time points (Figure S1-S2).

Similarly, propofol treatment was associated with a decrease in oncogenic miRNAs (miR-21 and miR-135a) and an increase in tumor-suppressive miRNAs (miR-34b and miR-98). These changes were observed both in propofol-treated groups and in the combination group, with more pronounced alterations in the

combination treatment compared with single treatments**,** indicating a sustained molecular response (Figure S3-S4).

Comparative analyses across HES and AN3CA cells revealed that the most pronounced and consistent expression changes occurred in mTOR, c-Myc, N-Cadherin, HMGB1, and MRP7/CFTR, leading to the selection of these targets for subsequent IF and IHC protein-level validation. Importantly, RT-qPCR analyses of tumor tissues showed expression patterns consistent with the *in vitro* findings, suggesting that similar molecular changes occur *in vivo* (Figure 3).

>Figure 3<

Adjuvant Propofol May Involve Carboplatin-Induced Suppression of Metastasis and Chemoresistance Pathways While Augmenting Apoptotic Signaling

Immunofluorescence analyses performed in HES and AN3CA cells demonstrated that treatment with Propofol, Carboplatin, or their combination significantly reduced the immunoreactivity of c-Myc (Figure 4A) and mTOR (Figure 4B) compared with controls. The lowest expression levels of both markers were consistently observed in the Carboplatin+Propofol group ($p<0.05$) (Figure 4C).

>Figure 4<

In parallel, the immunoreactivity of N-Cadherin (Figure 5A) and MRP7/CFTR (Figure 5B) was also significantly decreased following all treatments, with the most pronounced reduction detected in the Carboplatin+Propofol group, indicating that propofol is associated with increased carboplatin-related suppression of these proteins ($p<0.05$).

>Figure 5<

In contrast, HMGB1 expression was increased in all treatment groups, with the highest levels detected in the combination-treated group, suggesting a stronger combined effect rather than confirmed pharmacological synergy (Figure 6). Consistent with these findings, IF analyses revealed pronounced cytoplasmic loss in AN3CA cells treated with Carboplatin and combination treatment, whereas no comparable alterations were observed in HES cells, indicating differential effects between cell types rather than definitive tumor selectivity.

>Figure 6<

Immunohistochemical evaluation of tumor tissues further confirmed the *in vitro* results, showing a significant reduction in the immunoreactivity of c-Myc and mTOR (Figure 7A) in Propofol, Carboplatin, and combination-treated Type II EC xenografts compared with untreated tumors, with the most pronounced suppression observed in the Carboplatin+Propofol group (Figure 7B; $p<0.05$).

>Figure 7<

HMGB1 expression was markedly increased following combination therapy (Figure 8A). On the other hand, the immunoreactivity (Figure 8A) of N-Cadherin and MRP7/CFTR was significantly decreased in all treatment groups relative to controls (Figure 8B), with the greatest reduction detected in the Carboplatin+Propofol–treated xenografts ($p<0.05$).

>Figure 8<

Collectively, these data suggest that adjuvant propofol may be associated with carboplatin-related antitumoral and antimetastatic effects through changes in key proteins linked to chemoresistance and metastatic progression.

Histopathological Evidence of Adjuvant Propofol-Mediated Antitumoral and Antimetastatic Effects

Histopathological evaluation of tumor tissues using H&E staining revealed a marked increase in necrotic areas in all propofol-treated groups compared with untreated controls. Notably, combination therapy (Carboplatin+Propofol) resulted in more extensive tumor necrosis than carboplatin alone, accompanied by thinning or disruption of the tumor capsule, reduced tumor-associated adipose tissue, increased immune cell infiltration, and decreased neoangiogenic regions (Figure 8). Comparison between the Propofol and untreated Type II EC groups further demonstrated greater tumor necrosis and capsular thinning in propofol-treated tumors (Figure 9), showing a greater effect compared to the untreated group.

>Figure 9<

Histopathological analyses of distant organs showed that propofol treatment was associated with fewer observable metastatic foci in the lung and absence of detectable liver metastases under the conditions examined (Table 3). While no metastatic lesions were detected in animals treated with carboplatin alone, these specimens exhibited treatment-associated hemorrhage and edema. Importantly,

adjuvant propofol administration markedly attenuated these adverse histopathological changes. No metastatic lesions were observed in the brain or spleen in any experimental group (Figure 10).

>Figure 10<

Collectively, these findings suggest that propofol may be associated with reduced metastatic features; however, given that the evaluation was based on semi-quantitative histological assessment, these results should be interpreted with caution

Discussion

Among gynecological malignancies, EC represents one of the leading causes of cancer-related mortality, ranking after ovarian and cervical cancers [44]. Surgical resection remains the cornerstone of primary treatment and is frequently complemented by adjuvant chemotherapy to improve clinical outcomes [45]. Accumulating evidence over recent years indicates that anesthetic agents and anesthesia techniques used during cancer surgery may directly influence postoperative tumor recurrence and patient survival [26]. Numerous preclinical and clinical studies have demonstrated that anesthetics administered during oncological surgery can modulate key molecular regulators involved in neo-angiogenesis, epithelial–mesenchymal transition (EMT), and immune evasion, thereby affecting cancer cell proliferation, migration, invasion, and metastatic potential [26]. For instance, Du et al. reported that propofol suppresses proliferation, migration, and invasion while promoting apoptosis in EC cells through regulation of Sox4, a critical molecular driver of metastatic activity [29]. Similarly, Huang et al. demonstrated that propofol administered as an adjuvant to cisplatin enhanced chemosensitivity in human lung cancer cells [31]. These findings are highly consistent with the results obtained in the present study, which aimed to investigate—using molecular and histological approaches—the effects of propofol administered as an adjuvant to carboplatin on chemoresistance and metastasis in serous-type EC, both *in vitro* and *in vivo*. In the in vitro phase, MTT, wound-healing, and transwell migration assays revealed that propofol exerted a cytotoxic effect on Type II EC (AN3CA) cells. Notably, when combined with carboplatin, this effect was greater than either treatment alone, resulting in reduced cell proliferation and migratory capacity. *In vivo* findings also demonstrated that combination treatment was associated with a more pronounced reduction in tumor burden and semi-quantitatively assessed

metastatic features compared with single treatments. Collectively, these findings suggest that propofol may act as a potential adjuvant agent within the constraints of the semi-quantitative experimental assessments used in this study. This interpretation is further reinforced by the work of Wu and colleagues, who reported that propofol reduced tumor volume and inhibited proliferation, migration, and invasion in both *in vitro* and *in vivo* colorectal cancer models [46].

miRNAs are critical molecular regulators of essential cellular processes such as cell cycle progression, apoptosis, differentiation, and proliferation. In cancer, they may function either as tumor suppressors or oncogenes [47]. For example, the miR-34 family suppresses carcinogenesis and delays tumor progression by targeting more than 700 transcripts associated with proliferation, cellular survival, and plasticity [48]. In contrast, miR-21 has been shown to promote carcinogenesis and tumor progression in multiple cancer types through inhibition of the PTEN/PI3K/Akt signaling axis [49] . In EC, numerous studies have highlighted the close association between miRNA dysregulation and pathological processes such as metastasis, neo-angiogenesis, and chemoresistance. Wang et al. demonstrated that miR-135a enhances proliferation, migration, invasion, and chemoresistance in EC cells by modulating Akt signaling [17]. Similarly, Li et al. reported that miR-423 promotes chemoresistance by suppressing N-cadherin expression [18] (Li et al., 2018, while Sato et al. showed that miR-Let-7c contributes to paclitaxel resistance in EC by targeting Aurora B [19]. Conversely, several miRNAs—including miR-98, and miR-200c—have been shown to enhance chemosensitivity and exert anti-metastatic effects by targeting MRP-7, and TUBB3, respectively [23,24,50]. Additional studies have demonstrated that miR-1/133, miR-205, miR-449, and miR-34b suppress metastatic behavior by regulating PDE7A, mTOR, PTEN, and c-Myc expression [20–22].

Recent evidence further suggests that propofol promotes the expression of multiple tumor-suppressive miRNAs. Zhang et al. reported that propofol significantly upregulated miR-199a, thereby reducing invasive capacity in HepG2 cells [5]. Other studies have shown that propofol increases miR-133a and miR-328 expression in pancreatic cancer cells, leading to inhibition of proliferation, migration, and invasion [51,52]. In ovarian cancer, propofol has been reported to induce apoptosis and suppress growth and invasion through upregulation of miR-9 [53]. Conversely, propofol also exerts antitumor effects by suppressing oncogenic miRNAs, such as miR-21 in pancreatic cancer via inhibition of the miR-

21/Slug signaling pathway [54], and miR-374a in ovarian cancer, thereby reversing cisplatin resistance [55].

In the present study, RT-qPCR analyses of both AN3CA cells and tumors derived from xenograft EC models demonstrated downregulation of oncogenic miRNAs, including miR-21 and miR-135a, alongside upregulation of tumor-suppressive miRNAs such as miR-34b and miR-98. These findings are based on expression patterns and therefore indicate associations rather than direct regulatory interactions. When considered in conjunction with existing literature, these findings suggest that propofol treatment is associated with epigenetic changes that may contribute to its antitumor effects. Supporting this interpretation, IF and IHC analyses revealed significant suppression of pro-tumoral genes (mTOR, c-Myc, N-cadherin, and MRP7/CFTR) and concomitant upregulation of antitumoral genes (HMGB1 and PTEN) following propofol and/or carboplatin treatment

Notably, Huang et al. [23] demonstrated that miR-98-mediated downregulation of MRP7 reduces paclitaxel resistance in EC, which may a hypothesized explanatory framework for the observed changes in this study. In addition, Luan et al. reported that HMGB1 exerts antitumoral and anti-metastatic effects in EC via EMT inhibition [56], supporting the notion that increased HMGB1 expression observed here may be hypothetically associated with metastasis-related changes observed in this study. The observed downregulation of c-Myc, coupled with upregulation of miR-34b, may indicate a potential involvement of the miR-34b/c-Myc axis, although this relationship was not directly validated in the present study. Likewise, suppression of the miR-21/mTOR pathway—known to be closely associated with chemoresistance and metastasis—may represent a hypothesized mechanism underlying the observed effects [57]. Moreover, consistent with previous studies [58,59], the findings of the present study suggest that propofol increases caspase-3 activity in AN3CA cells and tumor tissues, thereby potentially contributing to increased apoptotic responses.

In addition to its antitumoral effects, histopathological analyses of brain, lung, liver, and spleen tissues revealed reduced hemorrhage and edema in mice treated with carboplatin plus propofol, suggesting a potential reduction in treatment-associated histopathological alterations under the conditions of this experimental model. This observation is consistent with previous reports demonstrating the neuroprotective effects of propofol in cisplatin-treated rodents [60]. Furthermore, analyses performed in HES cells showed higher cell viability in the carboplatin–

propofol combination group compared with carboplatin alone, further suggesting a differential response within the specific cell models used in this study. It should be noted that HES cells are stromal in origin, whereas AN3CA cells are epithelial tumor cells; therefore, comparisons between these models should be interpreted cautiously and are limited to the specific experimental conditions used in this study.

Overall, the integration of functional assays, molecular analyses, protein-level validation, and histopathological evaluation provides a coherent and biologically consistent framework indicating that propofol is associated with greater carboplatin efficacy in Type II EC, with observed changes in markers and features associated with metastasis and drug resistance within the experimental conditions of this study.

Conclusion

In conclusion, findings from both in vitro and in vivo components of this study suggest that propofol, when combined with carboplatin, is associated with greater antitumor and antimetastatic effects compared to either treatment alone. These effects are accompanied by changes in miRNA and gene expression profiles related to chemoresistance and metastasis.

However, as direct functional validation experiments were not performed, these observations should be interpreted as associative rather than mechanistic. Further studies incorporating targeted functional assays are required to clarify the underlying molecular mechanisms.

Limitations of The Study

Despite its comprehensive *in vitro* and *in vivo* design, this study has several limitations. Western blot analysis could not be performed due to technical constraints; however, protein-level validation was achieved through complementary immunofluorescence (IF) and immunohistochemistry (IHC) approaches, enabling evaluation of intracellular localization, relative protein abundance, and spatial expression patterns in tumor tissues. Although these techniques are semi-quantitative, the strong concordance between mRNA expression, protein alterations, and functional outcomes—including proliferation, migration, tumor growth, and metastasis—supports the proposed molecular mechanisms.

Formal drug interaction analyses, including dose–response modeling and combination index calculations, were not performed in present study. Therefore, although the combination treatment showed greater efficacy than single agents, pharmacological synergy cannot be concluded.

Additionally, mechanistic interpretations in this study are based on expression profiling and prior literature rather than direct experimental validation. miRNA–target gene interactions were inferred from observed expression patterns and previously reported findings, rather than being confirmed through gain- or loss-of-function approaches. Although existing evidence supports these associations, functional assays such as miRNA mimic/inhibitor experiments and luciferase reporter assays, along with high-throughput transcriptomic analyses, would be necessary to validate and further elucidate the proposed regulatory networks.

A further limitation is the reliance on a single Type II endometrial carcinoma model, AN3CA. This cell line is well characterized for its aggressive and chemoresistant phenotype, making it a relevant model; nevertheless, validation in additional cell lines or alternative models may increase generalizability. Due to budgetary and resource constraints, a second xenograft model could not be included. Moreover, HES cells were used as the normal control; these are stromal in origin, whereas AN3CA cells are epithelial. Therefore, conclusions regarding selective effects on tumor versus normal endometrial cells should be interpreted cautiously, and inclusion of a more appropriate non-malignant epithelial control would strengthen future studies. Despite these limitations, the findings provide preliminary evidence that can guide further investigation.

Overall, the integration of functional assays, molecular analyses, protein-level validation, and histopathological evaluation provides a coherent and biologically consistent framework indicating that propofol is associated with greater carboplatin efficacy in Type II EC, with observed changes in processes related to metastasis and drug resistance.

Author Contributions

İG, ÇG, and NY undertook the study design. ÇG, GCK, AB, and SÖAD undertook the animal experiments. AB and SÖAD undertook the histological experiments. NPÖ and HGK undertook the molecular experiments. ÇG, GCK, NY, NPÖ and İG assisted with the statistical analysis. GCK undertook the creation of graphs and figures. ÇG wrote the final manuscript. The manuscript was read and approved by all named authors.

Funding: This study was supported by The Scientific and Technological Research Council of Türkiye (TÜBİTAK) (Grant Number: 123S068 to İlkben Günüşen).

Data availability: The datasets generated during and/or analysed during the current study are available from the corresponding author on reasonable request.

Acknowledgments: The authors gratefully acknowledge the financial support provided by the Scientific and Technological Research Council of Türkiye (TÜBİTAK) for the conduct of this study.

Declarations

Competing Interests: The authors have no relevant financial or nonfinancial interests to disclose.

Ethics approval: This study was approved by the Ege University Animal Experimentation Local Ethics Committee (Approval Number: 2023-019; Approval Date: March 29, 2023), and was conducted in accordance with the Guide for the Care and Use of Laboratory Animals published by the National Institutes of Health. All procedures were conducted in accordance with the ARRIVE Guideline 2.0.

References

1. Anca-Stanciu, M.-B. B. *et al.* Comprehensive Review of Endometrial Cancer: New Molecular and FIGO Classification and Recent Treatment Changes. *J. Clin. Med.* **14,** 1385 (2025).
2. Gao, S., Wang, J., Li, Z., Wang, T. & Wang, J. Global Trends in Incidence and Mortality Rates of Endometrial Cancer Among Individuals Aged 55 years and Above From 1990 to 2021: An Analysis of the Global Burden of Disease. *Int. J. Womens. Health* **Volume 17,** 651–662 (2025).
3. Garg, V., Jayaraj, A. S. & Kumar, L. Novel approaches for treatment of endometrial carcinoma. *Curr. Probl. Cancer* **46,** 100895 (2022).
4. Menendez-Santos, M. *et al.* Endometrial Cancer: 2023 Revised FIGO Staging System and the Role of Imaging. *Cancers (Basel).* **16,** (2024).
5. Du, Q. *et al.* Propofol inhibits proliferation, migration, and invasion but promotes apoptosis by regulation of Sox4 in endometrial cancer cells. *Brazilian J. Med. Biol. Res.* **51,** (2018).
6. Legge, F. *et al.* Clinical outcome of recurrent endometrial cancer: analysis of post-relapse survival by pattern of recurrence and secondary treatment.

Int. J. Gynecol. Cancer **30,** 193–200 (2020).

7. Hicks, E., Shah, A. & Higgins, R. V. Therapeutic Challenges in the Management of Serous Endometrial Intraepithelial Carcinoma (SEIC). *Curr. Treat. Options Oncol.* **26,** 341–347 (2025).

8. Dinoi, G. *et al.* In search for biomarkers and potential drug targets for uterine serous endometrial cancer. *J. Cancer Res. Clin. Oncol.* **147,** 1647–1658 (2021).

9. Yan, L., Ding, X., Deng, Y., Li, Y. & Du, X. The molecular classification ushers in a new era for the treatment of advanced and recurrent endometrial cancer. *Front. Oncol.* **15,** (2026).

10. Svarna, A. *et al.* Molecular Prognostic Factors in Uterine Serous Carcinomas: A Systematic Review. *Curr. Oncol.* **32,** 251 (2025).

11. Niu, Z. *et al.* MTFR2 promotes endometrial carcinoma cell proliferation and growth via the miR-132-3p/PI3K/Akt signaling pathway. *Front. Med.* **11,** 1505071 (2025).

12. de Rooij, L. A. *et al.* The microRNA Lifecycle in Health and Cancer. *Cancers (Basel).* **14,** 5748 (2022).

13. Seyhan, A. A. Circulating microRNAs as Potential Biomarkers in Pancreatic Cancer—Advances and Challenges. *Int. J. Mol. Sci.* **24,** 13340 (2023).

14. Favier, A. *et al.* MicroRNA as Epigenetic Modifiers in Endometrial Cancer: A Systematic Review. *Cancers (Basel).* **13,** 1137 (2021).

15. Bogaczyk, A. *et al.* The Role of miRNAs in the Development, Proliferation, and Progression of Endometrial Cancer. *Int. J. Mol. Sci.* **24,** 11489 (2023).

16. Zhao, W., Geng, P., Li, Y., Wei, X. & Cheng, J. MicroRNA-21 promotes endometrial carcinoma proliferation and invasion by targeting PTEN. *Int. J. Clin. Exp. Pathol.* **10,** 11489 (2017).

17. Wang, J. *et al.* MicroRNA-135a promotes proliferation, migration, invasion and induces chemoresistance of endometrial cancer cells. *Eur. J. Obstet. Gynecol. Reprod. Biol. X* **5,** 100103 (2020).

18. Li, J., Sun, H., Liu, T. & Kong, J. MicroRNA-423 promotes proliferation, migration and invasion and induces chemoresistance of endometrial cancer cells. *Exp. Ther. Med.* **16,** 4213–4224 (2018).

19. Sato, I. *et al.* MicroRNA Let-7c Contributes to Paclitaxel Resistance via Aurora-B in Endometrial Serous Carcinoma. *Tohoku J. Exp. Med.* **251,** 263–272 (2020).

20. Yamamoto, N. *et al.* The tumor-suppressive microRNA-1/133a cluster targets PDE7A and inhibits cancer cell migration and invasion in endometrial cancer. *Int. J. Oncol.* **47,** 325–334 (2015).

21. Meng, H. *et al.* MiR-449a regulates the cell migration and invasion of human non-small cell lung carcinoma by targeting ADAM10. *Onco. Targets. Ther.* **12,** 3829 (2019).

22. Yanokura, M., Banno, K. & Aoki, D. MicroRNA-34b expression enhances chemosensitivity of endometrial cancer cells to paclitaxel. *Int. J. Oncol.* **57,** 1145–1156 (2020).

23. Huang, W. *et al.* A Novel miR-98 Negatively Regulates the Resistance of Endometrial Cancer Cells to Paclitaxel by Suppressing ABCC10/MRP-7. *Front. Oncol.* **11,** 5098 (2021).

24. Cochrane, D. R., Spoelstra, N. S., Howe, E. N., Nordeen, S. K. & Richer, J. K. MicroRNA-200c mitigates invasiveness and restores sensitivity to microtubule-targeting chemotherapeutic agents. *Mol. Cancer Ther.* **8,** 1055–1066 (2009).

25. Kazi, M. *et al.* Propofol: Current Updates, Challenges, and Strategies for Improved Self-Nanoemulsifying Formulation. *ACS Pharmacol. Transl. Sci.* **8,** 1013–1027 (2025).

26. Choi, H. & Hwang, W. Anesthetic Approaches and Their Impact on Cancer Recurrence and Metastasis: A Comprehensive Review. *Cancers (Basel).* **16,** 4269 (2024).

27. Jiang, S., Liu, Y., Huang, L., Zhang, F. & Kang, R. Effects of propofol on cancer development and chemotherapy: Potential mechanisms. *Eur. J. Pharmacol.* **831,** 46–51 (2018).

28. Zhang, Y. F., Li, C. S., Zhou, Y. & Lu, X. H. Propofol facilitates cisplatin sensitivity via lncRNA MALAT1/miR-30e/ATG5 axis through suppressing autophagy in gastric cancer. *Life Sci.* **244,** 117280 (2020).

29. Du, Q. H., Xu, Y. B., Zhang, M. Y., Yun, P. & He, C. Y. Propofol induces apoptosis and increases gemcitabine sensitivity in pancreatic cancer cells

in vitro by inhibition of nuclear factor-κB activity. *World J. Gastroenterol.* **19,** 5485 (2013).

30. Wang, P. *et al.* Propofol inhibits invasion and enhances paclitaxel-induced apoptosis in ovarian cancer cells through the suppression of the transcription factor slug (European review for medical and pharmacological sciences (2013) 17 13 (1722-1729) PII: 27139). *Eur. Rev. Med. Pharmacol. Sci.* **25,** 6446 (2021).

31. Huang, Y., Lei, L. & Liu, Y. Propofol Improves Sensitivity of Lung Cancer Cells to Cisplatin and Its Mechanism. *Med. Sci. Monit.* **26,** e919786-1 (2020).

32. Pectasides, D. *et al.* Carboplatin and paclitaxel in advanced or metastatic endometrial cancer. *Gynecol. Oncol.* **109,** 250–254 (2008).

33. Tirmazy, S. H., Barthakur, U., El-Modir, A., Anwar, S. & Fernando, I. Chemotherapy for advanced endometrial cancer with carboplatin and epirubicin. *Anticancer Res.* **34,** 3793–3798 (2014).

34. Korets, S. B., Musa, F., Curtin, J., Blank, S. V. & Schneider, R. J. Dual mTORC1/2 inhibition in a preclinical xenograft tumor model of endometrial cancer. *Gynecol. Oncol.* **132,** 468–473 (2014).

35. Moskot, M. *et al.* The Role of Dimethyl Sulfoxide (DMSO) in Gene Expression Modulation and Glycosaminoglycan Metabolism in Lysosomal Storage Disorders on an Example of Mucopolysaccharidosis. *Int. J. Mol. Sci.* **20,** 304 (2019).

36. Fan, Y. *et al.* NLRC5 promotes cell migration and invasion by activating the PI3K/AKT signaling pathway in endometrial cancer. *J. Int. Med. Res.* **48,** 1–13 (2020).

37. Grada, A., Otero-Vinas, M., Prieto-Castrillo, F., Obagi, Z. & Falanga, V. Research Techniques Made Simple: Analysis of Collective Cell Migration Using the Wound Healing Assay. *J. Invest. Dermatol.* **137,** e11–e16 (2017).

38. Shen, J. *et al.* The E3 ubiquitin ligase TRIM17 promotes gastric cancer survival and progression via controlling BAX stability and antagonizing apoptosis. *Cell Death Differ.* **30,** 2322–2335 (2023).

39. Jiang, F. *et al.* MiR-125b promotes proliferation and migration of type II endometrial carcinoma cells through targeting TP53INP1 tumor suppressor

in vitro and in vivo. *BMC Cancer* **11,** 425 (2011).

40. Kwak, Y., Cho, H., Hur, W. & Sim, T. Antitumor effects and mechanisms of AZD4547 on FGFR2-deregulated endometrial cancer cells. *Mol. Cancer Ther.* **14,** 2292–2302 (2015).

41. Qiu, M. T. *et al.* KDM4B and KDM4A promote endometrial cancer progression by regulating androgen receptor, c-myc, and p27kip1. *Oncotarget* **6,** 31702 (2015).

42. Friel, A. M. *et al.* Progesterone receptor membrane component 1 deficiency attenuates growth while promoting chemosensitivity of human endometrial xenograft tumors. *Cancer Lett.* **356,** 434–442 (2015).

43. Young, K. & Morrison, H. Quantifying Microglia Morphology from Photomicrographs of Immunohistochemistry Prepared Tissue Using ImageJ. *J. Vis. Exp.* (2018). doi:10.3791/57648

44. Ramírez, S. P. *et al.* SEOM-GEICO clinical guidelines on endometrial cancer (2025). *Clin. Transl. Oncol.* **27,** 4368–4380 (2025).

45. Pagano, F. *et al.* Intraoperative Radiation Therapy for Gynecologic Malignancies: When Is It Indicated? *Cancers (Basel).* **17,** 1240 (2025).

46. Wu, Z., Wang, H., Shi, Z.-A. & Li, Y. Propofol Prevents the Growth, Migration, Invasion, and Glycolysis of Colorectal Cancer Cells by Downregulating Lactate Dehydrogenase Both In Vitro and In Vivo. *J. Oncol.* **2022,** 1–11 (2022).

47. Zoroddu, S., Sias, F. & Bagella, L. The Double Life of microRNAs in Bone Sarcomas: Oncogenic Drivers and Tumor Suppressors. *Int. J. Mol. Sci.* **26,** (2025).

48. Slabáková, E., Culig, Z., Remšík, J. & Souček, K. Alternative mechanisms of miR-34a regulation in cancer. *Cell Death Dis.* **8,** e3100–e3100 (2017).

49. Chawra, H. S. *et al.* MicroRNA-21's role in PTEN suppression and PI3K/AKT activation: Implications for cancer biology. *Pathol. Res. Pract.* **254,** 155091 (2024).

50. Ran, X. *et al.* MiR-218 inhibits HMGB1-mediated autophagy in endometrial carcinoma cells during chemotherapy. *Int. J. Clin. Exp. Pathol.* **8,** 6617–6626 (2015).

51. Wang, Z. T., Gong, H. Y., Zheng, F., Liu, D. J. & Dong, T. L. Propofol suppresses proliferation and invasion of pancreatic cancer cells by upregulating microRNA-133a expression. *Genet. Mol. Res.* **14,** 7529–7537 (2015).

52. Yu, X., Gao, Y. & Zhang, F. Propofol inhibits pancreatic cancer proliferation and metastasis by up-regulating miR-328 and down-regulating ADAM8. *Basic Clin. Pharmacol. Toxicol.* **125,** 271–278 (2019).

53. Huang, X., Teng, Y., Yang, H. & Ma, J. Propofol inhibits invasion and growth of ovarian cancer cells via regulating miR-9/NF-κB signal. *Brazilian J. Med. Biol. Res.* **49,** e5717 (2016).

54. Liu, Z. *et al.* Propofol inhibits growth and invasion of pancreatic cancer cells through regulation of the miR-21/Slug signaling pathway. *Am. J. Transl. Res.* **8,** 4120–4133 (2016).

55. Sun, Y. *et al.* Propofol inhibits proliferation and cisplatin resistance in ovarian cancer cells through regulating the microRNA-374a/forkhead box O1 signaling axis. *Mol. Med. Rep.* **21,** 1471–1480 (2020).

56. Luan, X., Ma, C., Wang, P. & Lou, F. HMGB1 is negatively correlated with the development of endometrial carcinoma and prevents cancer cell invasion and metastasis by inhibiting the process of epithelial-to-mesenchymal transition. *Onco. Targets. Ther.* **Volume 10,** 1389–1402 (2017).

57. Zhuo, Z. & Yu, H. miR-205 inhibits cell growth by targeting AKT-mTOR signaling in progesterone-resistant endometrial cancer Ishikawa cells. *Oncotarget* **8,** 28042–28051 (2017).

58. Sun, C., Liu, P., Pei, L., Zhao, M. & Huang, Y. Propofol Inhibits Proliferation and Augments the Anti-Tumor Effect of Doxorubicin and Paclitaxel Partly Through Promoting Ferroptosis in Triple-Negative Breast Cancer Cells. *Front. Oncol.* **12,** 837974 (2022).

59. Hu, X., Hu, X. & Wang, Q. Propofol induces apoptosis of hepatocellular carcinoma cells by upregulating miR-134 expression. *Transl. Cancer Res.* **10,** 3004–3012 (2021).

60. Gonullu, E., Dagistan, G., Erkin, Y., Erdogan, M. A. & Erbas, O. Demonstration of the protective effect of propofol in rat model of cisplatin-

induced neuropathy. *Bratisl. Lek. Listy* **124,** 64–69 (2023).

61. Lakics, V., Karran, E. H. & Boess, F. G. Quantitative comparison of phosphodiesterase mRNA distribution in human brain and peripheral tissues. *Neuropharmacology* **59,** 367–374 (2010).

62. Lin, Y. S. *et al.* Gene Expression Profiles of the Aurora Family Kinases. *Gene Expr.* **13,** 15 (2006).

63. Ioffe, Y. J., Chiappinelli, K. B., Mutch, D. G., Zighelboim, I. & Goodfellow, P. J. Phosphatase and tensin homolog (PTEN) pseudogene expression in endometrial cancer: a conserved regulatory mechanism important in tumorigenesis? *Gynecol. Oncol.* **124,** 340 (2012).

64. Kumar, N., Basundra, R. & Maiti, S. Elevated polyamines induce c-MYC overexpression by perturbing quadruplex–WC duplex equilibrium. *Nucleic Acids Res.* **37,** 3321 (2009).

65. Kotzamanis, G. *et al.* CFTR expression from a BAC carrying the complete human gene and associated regulatory elements. *J. Cell. Mol. Med.* **13,** 2938 (2009).

66. Zhang, J., Zhang, L. L., Shen, L., Xu, X. M. & Yu, H. G. Regulation of AKT gene expression by cisplatin. *Oncol. Lett.* **5,** 756 (2013).

67. Riquelme, I. *et al.* The Gene Expression Status of the PI3K/AKT/mTOR Pathway in Gastric Cancer Tissues and Cell Lines. *Pathol. Oncol. Res.* **22,** 797 (2016).

68. Wu, C. *et al.* Evaluation of high mobility group box 1 protein as a presurgical diagnostic marker reflecting the severity of acute appendicitis. *Scand. J. Trauma. Resusc. Emerg. Med.* **20,** 61 (2012).

69. Shibazaki, M. *et al.* Transcriptional and post-transcriptional regulation of βIII-tubulin protein expression in relation with cell cycle-dependent regulation of tumor cells. *Int. J. Oncol.* **40,** 695–702 (2012).

70. Sun, H. *et al.* Overexpression of N-cadherin and β-catenin correlates with poor prognosis in patients with nasopharyngeal carcinoma. *Oncol. Lett.* **13,** 1725 (2017).

71. Sun, L. *et al.* Expression of circulating microRNA-1 and microRNA-133 in pediatric patients with tachycardia. *Mol. Med. Rep.* **11,** 4039 (2015).

72. Liu, G. X. *et al.* Hsa-let-7c controls the committed differentiation of IGF-1-treated mesenchymal stem cells derived from dental pulps by targeting IGF-1R via the MAPK pathways. *Exp. Mol. Med. 2018 504* **50,** 1–14 (2018).

73. Yan, F., Wang, C., Li, T., Cai, W. & Sun, J. Role of miR-21 in the growth and metastasis of human salivary adenoid cystic carcinoma. *Mol. Med. Rep.* **17,** 4237–4244 (2018).

74. Yang, H. *et al.* miR-20b-5p functions as tumor suppressor microRNA by targeting cyclinD1 in colon cancer. *Cell Cycle* **19,** 2939–2954 (2020).

75. Zhuang, X.-F. *et al.* miR-34b inhibits the migration/invasion and promotes apoptosis of non-small-cell lung cancer cells by YAF2. *Eur. Rev. Med. Pharmacol. Sci.* **23,** 2038–2046 (2019).

76. Zhu, Y. *et al.* miR-98-5p Alleviated Epithelial-to-Mesenchymal Transition and Renal Fibrosis via Targeting Hmga2 in Diabetic Nephropathy. *Int. J. Endocrinol.* **2019,** 4946181 (2019).

77. Chen, Y. *et al.* MiRNA-135a promotes breast cancer cell migration and invasion by targeting HOXA10. *BMC Cancer* **12,** 1–11 (2012).

78. Liu, Z., Mao, L., Wang, L., Zhang, H. & Hu, X. miR-218 functions as a tumor suppressor gene in cervical cancer. *Mol. Med. Rep.* **21,** 209 (2020).

79. Wang, C., Kang, L., Wang, X., Liu, Y. & Zhao, X. Expression of miR-200a and chemotherapeutic treatment efficacy of glioma. *Oncol. Lett.* **15,** 5767 (2018).

80. Liu, J. *et al.* Upregulation of miR-205 induces CHN1 expression, which is associated with the aggressive behaviour of cervical cancer cells and correlated with lymph node metastasis. *BMC Cancer* **20,** 1029 (2020).

Tables and Figures

Table 1. The primer antibodies used in IF and IHC analyses

Table 2. RT-qPCR primer sequences for target genes and miRNAs

Antibody	Catalog No/Manufacturer	Dilution ratio IF/IHC
Cleaved Caspase-3	25128-1-AP-150UL/Proteintech, Manchester, UK	-/1:200
c-Myc	10828-1-AP-150UL /Proteintech, Manchester, UK	1:800/1:500
HMGB1	10829-1-AP-150UL / Proteintech, Manchester, UK	1:500/1:200
MRP7/CTFR	20738-1-AP-150UL / Proteintech, Manchester, UK	1:250/1:250
mTOR	28273-1-AP-150UL / Proteintech, Manchester, UK	1:250/1:100
N-Cadherin	22018-1-AP-150UL / Proteintech, Manchester, UK	1:200/1:2000

Gene/miRNA	RT-qPCR Primer Sequences	Reference
PDE7A	Forward: 5’- AGATAGGTGCTCTGATACTAG -3’ Reverse: 5’- ATGTCTGTGTCTGGTGTC -3’	[61]
Aurora B	Forward: 5’- GGCGCATGCACAATGAGA -3’ Reverse: 5’- TCCCCACCAGCAGCTCATAG -3’	[62]
PTEN	Forward: 5'- CCTTCTCCATCTCCTGTGTAATCAA -3’ Reverse: 5'- GTTGACTGATGTAGGTACTAACAGCAT -3’	[63]
c-Myc	Forward: 5’- TGAGGAGACACCGCCCAC -3’ Reverse: 5’- CAACATCGATTTCTTCCTCATCTTC -3’	[64]
MRP-7/CTFR	Forward: 5’- GTTGGCATTCCAGCATTGCTT -3’ Reverse: 5’- ACGTGAAGAAAGATGACATC -3’	[65]
AKT	Forward: 5’- TCTATGGCGCTGAGATTGTG -3’ Reverse: 5’- CTTAATGTGCCCGTCCTTGT -3’	[66]
mTOR	Forward: 5’- GCTTGATTTGGTTCCCAGGACAGT -3’ Reverse: 5’- GTGCTGAGTTTGCTGTACCCATGT -3’	[67]
HMGB1	Forward: 5’- GCGGACAAGGCCCGTTA -3’ Reverse: 5’- AGAGGAAGAAGGCCGAAGGAA -3’	[68]
TUBB3	Forward: 5’- GGGCCAAGTTCTGGGAAGTC -3’ Reverse: 5’- AGTCGCCCACGTAGTTGCC -3’	[69]
N-Cadherin	Forward: 5’- GCGTCTGTAGAGGCTTCTGG -3’ Reverse: 5’- GCCACTTGCCACTTTTCCTG-3’	[70]
Aktin (Reference)	Forward: 5’- CACGATGGAGGGGCCGGACTCATC -3’ Reverse: 5’- TAAAGACCTCTATGCCAACACAGT -3’	[66]

miR-1	Forward: 5’- ACACTCCAGCTGGGTGGAATGTAAAGAAGT -3’ Reverse: 5’- TCAACTGGTGTCGTGGAGTCGGCAATTCTTGAGCAGCTGGT -3’	[71]
miR-133	Forward: 5’- ACACTCCAGCTGGGTTTGGTCCCCTTCAAC -3’ Reverse: 5’- CTCAACTGGTGTCGTGGAGTCGGC -3’	[71]
Let-7c	Forward: 5’- ACACTCCAGCTGGGTGAGGTAGTAGGTTGT -3’ Reverse: 5’- TGGTGTCGTGGAGTCG -3’	[72]
miR-21	Forward: 5’- GTCGTATCCAGTGCAGGGT-3’ Reverse: 5’- CCAGTGCAGGGTCCGAGGTATT -3’	[73]
miR-20b	Forward: 5’- ACACTCCAGCTGGGCAAAGTGCTCATAGT -3’ Reverse: 5’- TGGTGTCGTGGAGTCG-3’	[74]
miR34b	Forward: 5’- TCTATTTGCCATCGTCTA -3’ Reverse: 5’- CAGGCAGCTCATTTGGAC -3’	[75]
miR-98	Forward: 5’- ATCCAGTGCGTGTCGTG -3’ Reverse: 5’- TGCTTGAGGTAGTAAGTTG -3’	[76]
miR-135a	Forward: 5’- CGCGTCTATGGCTTTTTATTCCTA -3’ Reverse: 5’- CCAGTCTCAGGGTCCGAGGTATTC -3’	[77]
miR-218	Forward: 5’- CGAGTGCATTTGTGCTTGATCTA -3’ Reverse: 5’- TGGTGTCGTGGAGTCG -3’	[78]
miR-200a	Forward: 5’- TAACACTGTCTGGTAACGATGT -3’ Reverse: 5’- ATCGTTACCAGACAGTGTTATT -3’	[79]
miR-205	Forward: 5’- AATTGTCCTTCATTCCACCGG -3’ Reverse: 5’- GTGCAGGGTCCGAGGT -3’	[80]
miR-423	Forward: 5’- GCCTGAGGCGCAGAGAGC- -3’ Reverse: 5’- CCACGTGTCGTGGAGTC -3’	[18]
miR-449	Forward: 5’- TGGCAGTGTATTGTTA- -3’ Reverse: 5’- ATCCAGTGCAGGGTCCGAGG -3’	[21]
U6 (Reference)	Forward: 5’- CTCGCTTCGGCAGCACA -3’ Reverse: 5’- AACGCTTCACGAATTTGCGT -3’	[76]

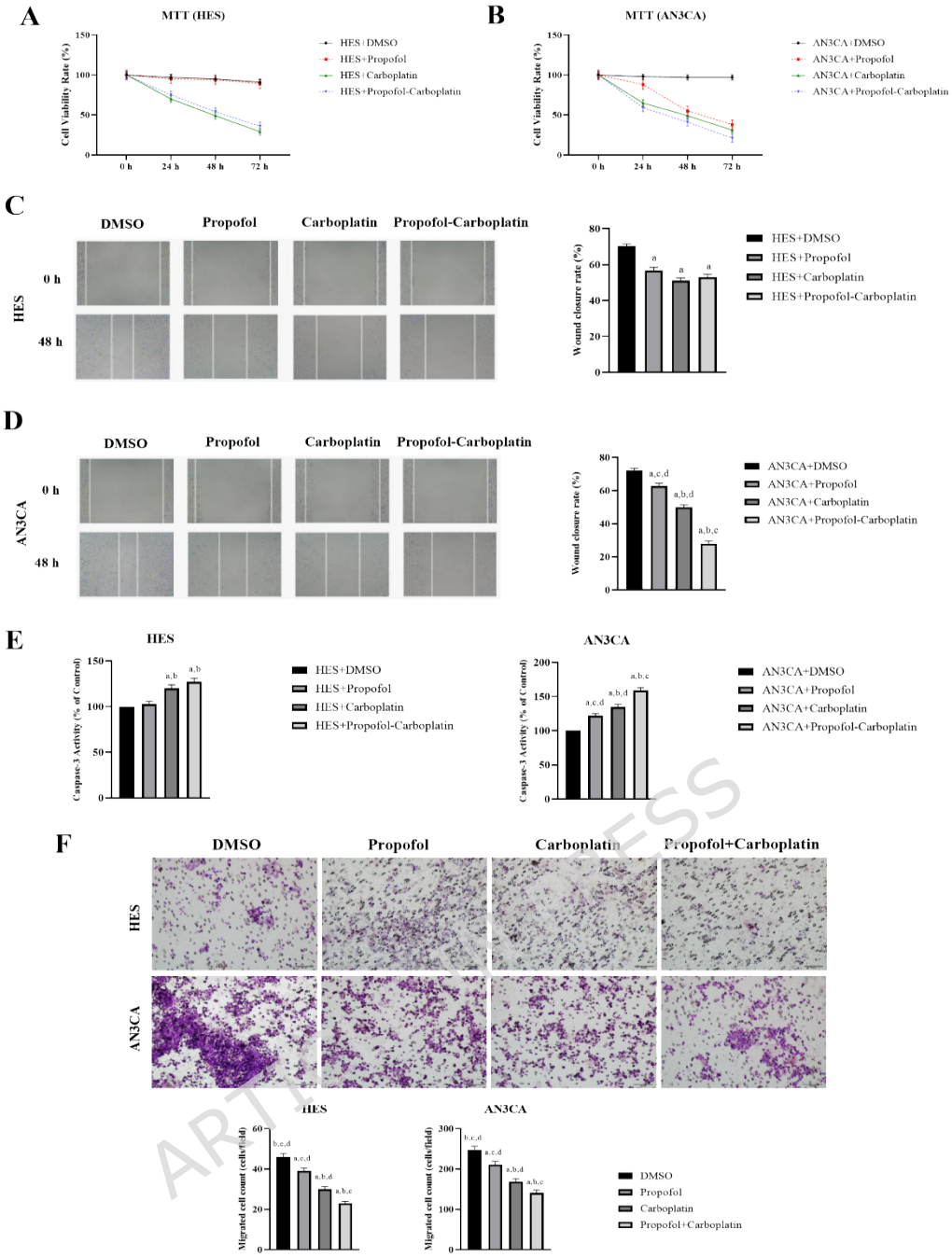

Figure 1. Effects of propofol and carboplatin, alone or in combination, on cell viability, proliferation, apoptosis, and migration in HES and AN3CA cells. MTT assays (Figure 1A) showed that propofol did not significantly affect HES cell proliferation, whereas carboplatin markedly reduced cell viability at all time points; this cytotoxic effect was partially attenuated by combined treatment. In contrast, propofol significantly decreased AN3CA cell viability at 24, 48, and 72 h, with pronounced pro-apoptotic effects observed at 72 h. Adjuvant propofol significantly enhanced the antiproliferative and apoptotic effects of carboplatin in AN3CA cells, reducing viability to approximately 20% at 72 h. Wound healing (Figure 1C–D), Caspase-3 activity (Figure 1E) and transwell migration assays (Figure 1F) further demonstrated that propofol significantly inhibited AN3CA cell migration and promoted apoptosis in these cells, an effect that was stronger with carboplatin and most pronounced under combination treatment. $p<0.05$ versus control. a: Significant change compared to DMSO group ($p<0.05$); b: Significant change compared to propofol group ($p<0.05$); c: Significant change compared to carboplatin group ($p<0.05$); d: Significant change compared to propofol-carboplatin group ($p<0.05$). Low-magnification images are shown in the upper panels (scale bar: 100 μm), whereas high-magnification images are presented in the lower panels (scale bar: 20 μm). Data represent mean ± SD of n = 3 independent experiments, each performed in triplicate. Statistical analyses were performed using two-way ANOVA followed by

Tukey’s post hoc test for panels (A–D), and one-way ANOVA followed by Tukey’s post hoc test for panels (E–F).

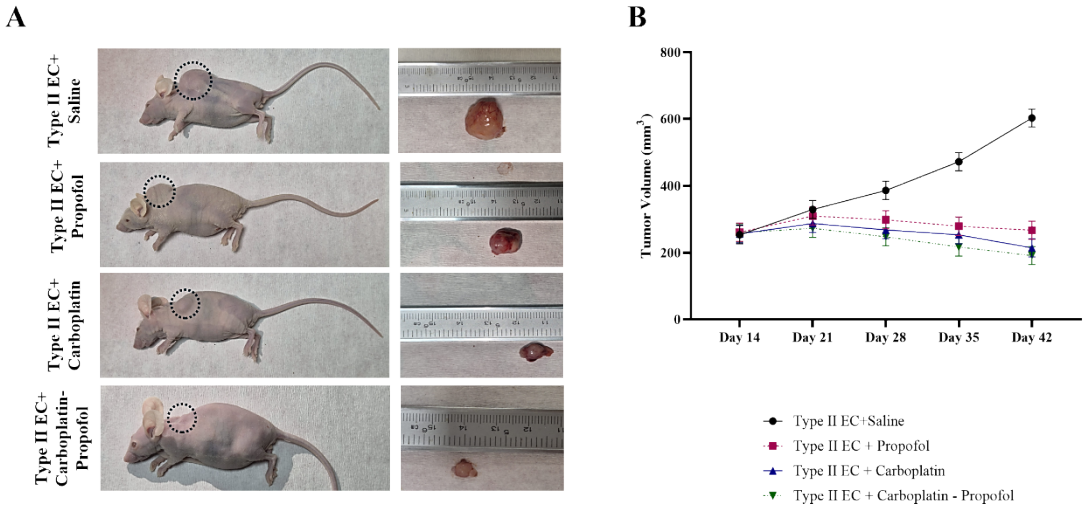

Figure 2. *In vivo* effects of propofol and carboplatin on tumor growth in Type II EC xenografts. Untreated xenografts displayed progressive tumor growth throughout the observation period (Figure 2A). In contrast, significant tumor regression was detected from day 21 onward in the Propofol-, Carboplatin-, and combination-treated groups (Figure 2B), with the greatest reduction in tumor volume observed in the Propofol–Carboplatin combination group ($p<0.05$). Data represent mean ± SD of n = 10. Statistical significance was determined using two-way ANOVA followed by Tukey's post-hoc test.

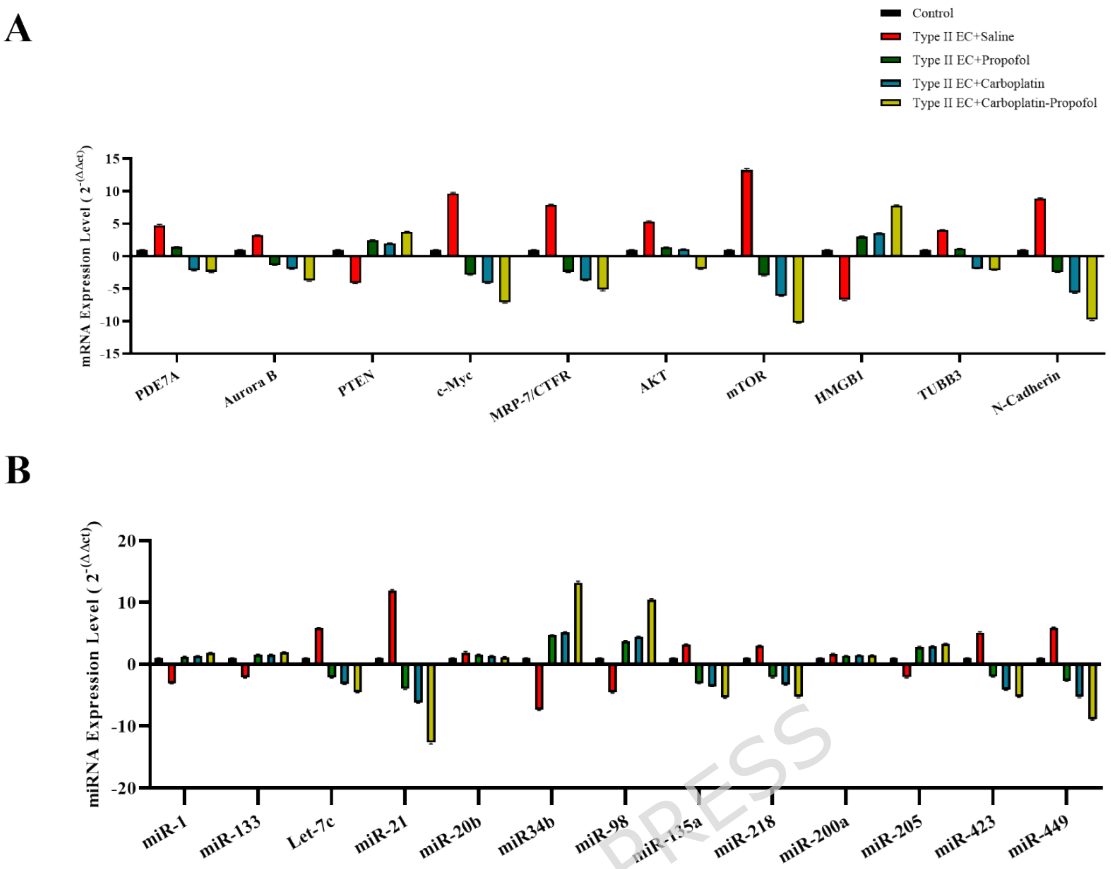

Figure 3. RT-qPCR analysis of tumor tissues from Type II EC xenografts following propofol and carboplatin treatment. Gene expression profiling demonstrates treatment-associated molecular changes consistent with antitumoral and antimetastatic reprogramming, with propofol alone and in combination with carboplatin producing expression patterns that parallel those observed *in vitro*.

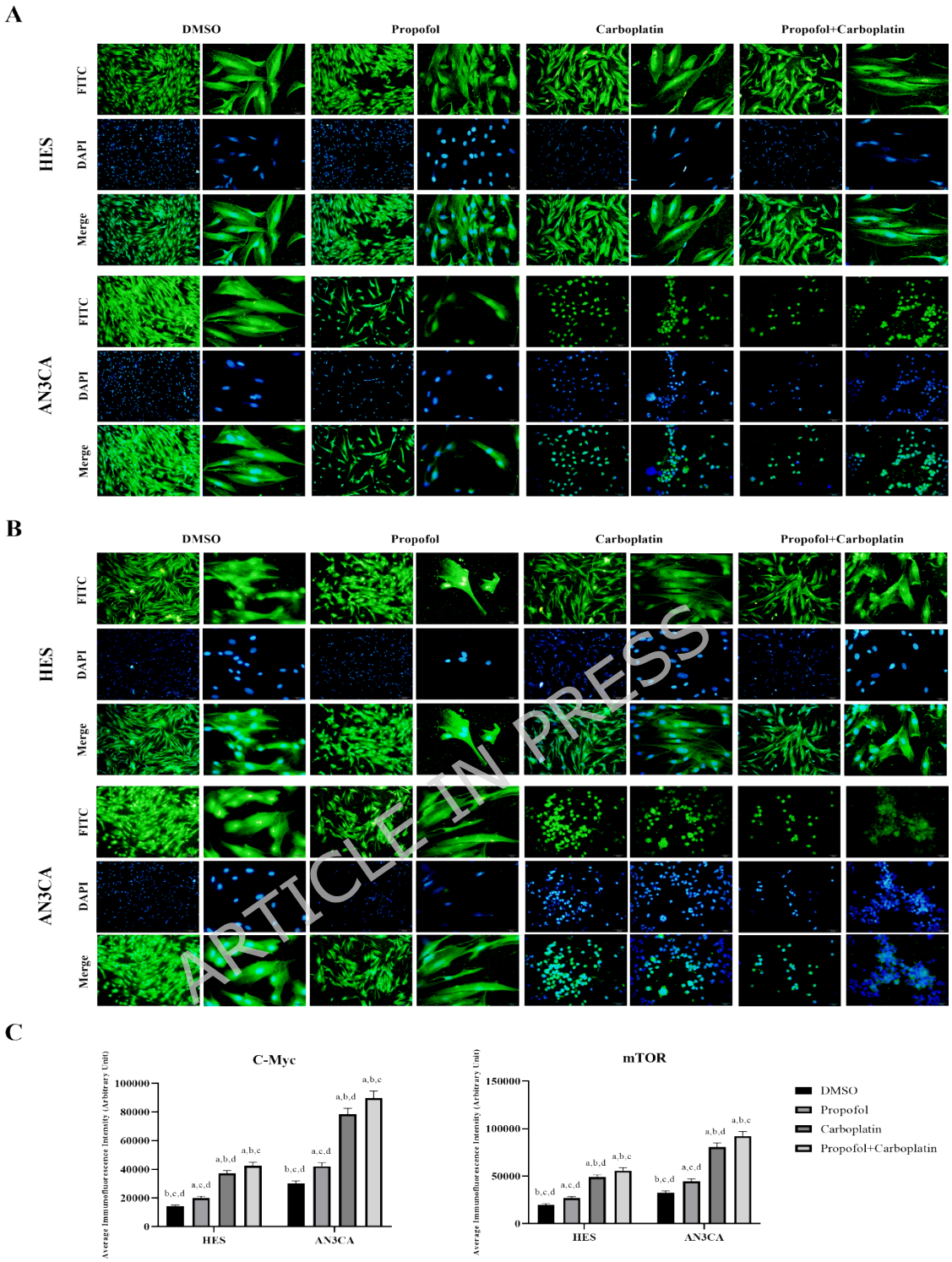

Figure 4. Immunofluorescence analysis of c-Myc and mTOR expression in HES and AN3CA cells following treatment with propofol and carboplatin. Representative images illustrate decreased c-Myc and mTOR immunoreactivity in cells treated with propofol, carboplatin, or their combination compared with controls, with low-magnification views shown in the left panels (scale bar: 100 μm) and high-magnification views in the right panels (scale bar: 20 μm) (Figure 4A-B). Quantitative analysis confirmed that combined Propofol–Carboplatin treatment resulted in the lowest expression levels of both markers among all groups (Figure 4C; $p<0.05$).*a*: significant change compared to DMSO group ($p<0.05$); *b*: significant change compared to propofol group ($p<0.05$); *c*: significant change compared to carboplatin group ($p<0.05$); *d*: significant change compared to propofol–carboplatin group ($p<0.05$). Data represent mean ± SD of n = 3 independent experiments, each

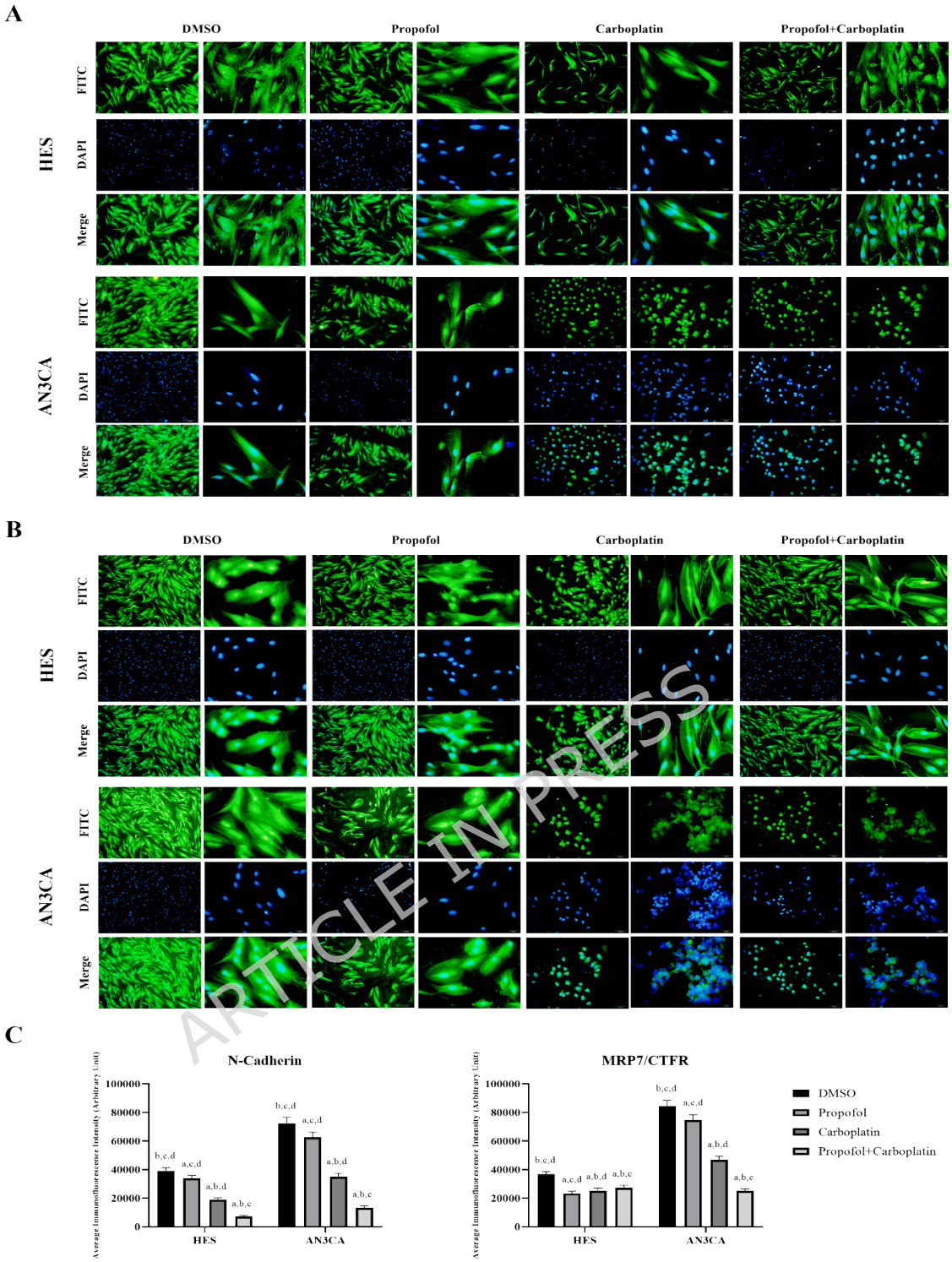

performed in triplicate. Statistical significance was determined using one-way ANOVA followed by Tukey's post-hoc test.

Figure 5. Immunofluorescence analysis of N-Cadherin and MRP7/CFTR expression in HES and AN3CA cells after propofol and carboplatin exposure. Representative micrographs demonstrate reduced immunoreactivity of N-Cadherin and MRP7/CFTR (Figure 5A–B) across all treatment groups compared with controls, with low-magnification images shown in the left panels (scale bar: 100 µm) and high-magnification images in the right panels (scale bar: 20 µm). Quantitative assessment indicates that combined Propofol–Carboplatin treatment resulted in the greatest decrease in fluorescence intensity for both markers, consistent with greater suppression of metastasis- and chemoresistance-associated protein expression compared with single treatments.

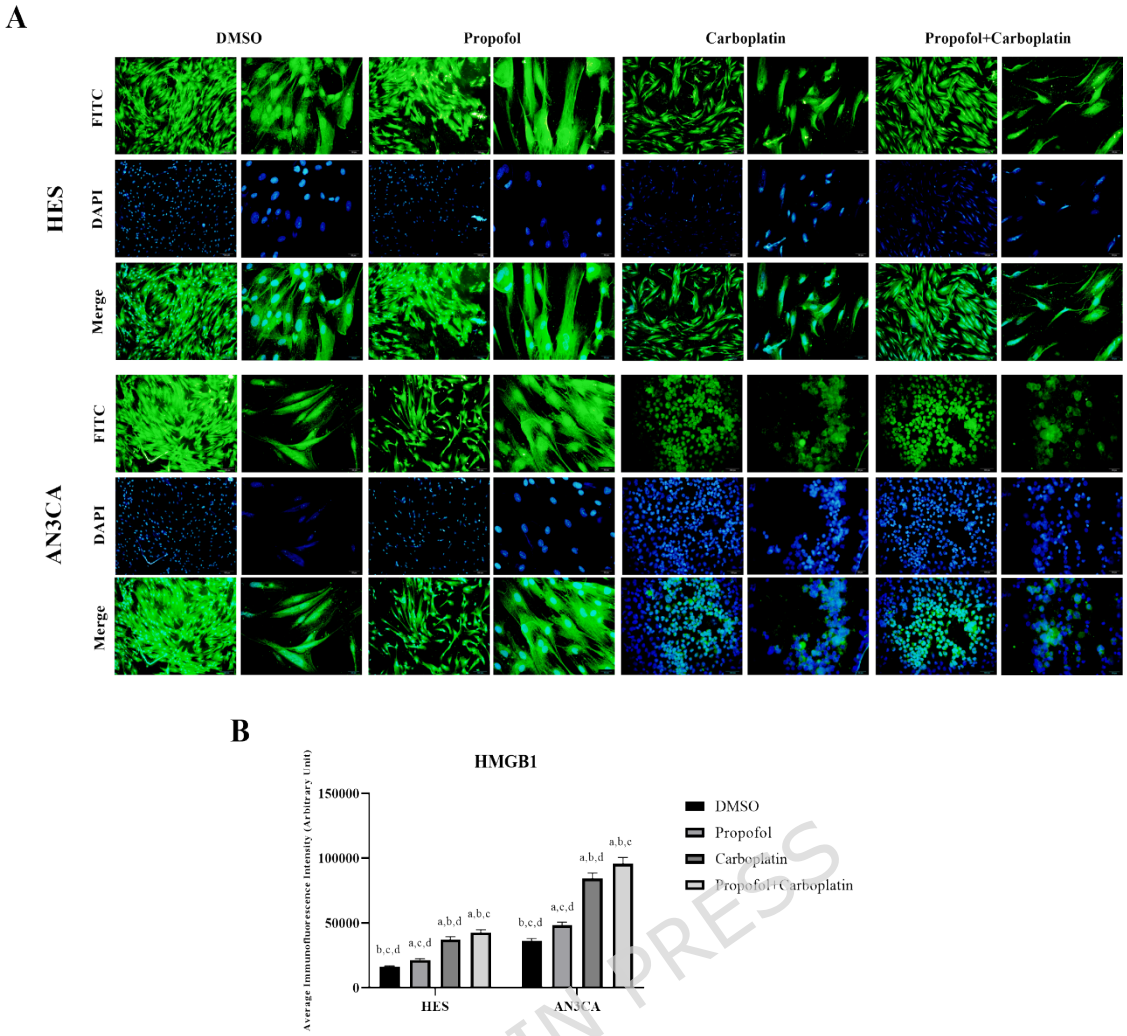

a: significant change compared to DMSO group ($p<0.05$); *b*: significant change compared to propofol group ($p<0.05$); *c*: significant change compared to carboplatin group ($p<0.05$); *d*: significant change compared to propofol–carboplatin group ($p<0.05$). Data represent mean ± SD of n = 3 independent experiments, each performed in triplicate. Statistical significance was determined using one-way ANOVA followed by Tukey's post-hoc test.

Figure 6. HMGB1 expression and intracellular localization following propofol and carboplatin treatment. Immunofluorescence images illustrate increased HMGB1 immunoreactivity in treated groups compared with controls, with the strongest signal observed following combined Propofol–Carboplatin treatment (Figure 6A–B). Representative low-magnification images are shown in the left panels (scale bar: 100 µm), and corresponding high-magnification images are shown in the right panels (scale bar: 20 µm). In AN3CA cells, carboplatin alone and in combination with propofol was associated with a marked reduction in cytoplasmic HMGB1 staining, whereas no comparable alterations were observed in normal endometrial HES cells (Figure 6C; $p<0.05$). *a*: significant change compared to DMSO group ($p<0.05$); *b*: significant change compared to propofol group ($p<0.05$); *c*: significant change compared to carboplatin group ($p<0.05$); *d*: significant change compared to propofol–carboplatin group ($p<0.05$). Data represent mean ± SD of n = 3 independent experiments, each performed in triplicate. Statistical significance was determined using one-way ANOVA followed by Tukey's post-hoc test.

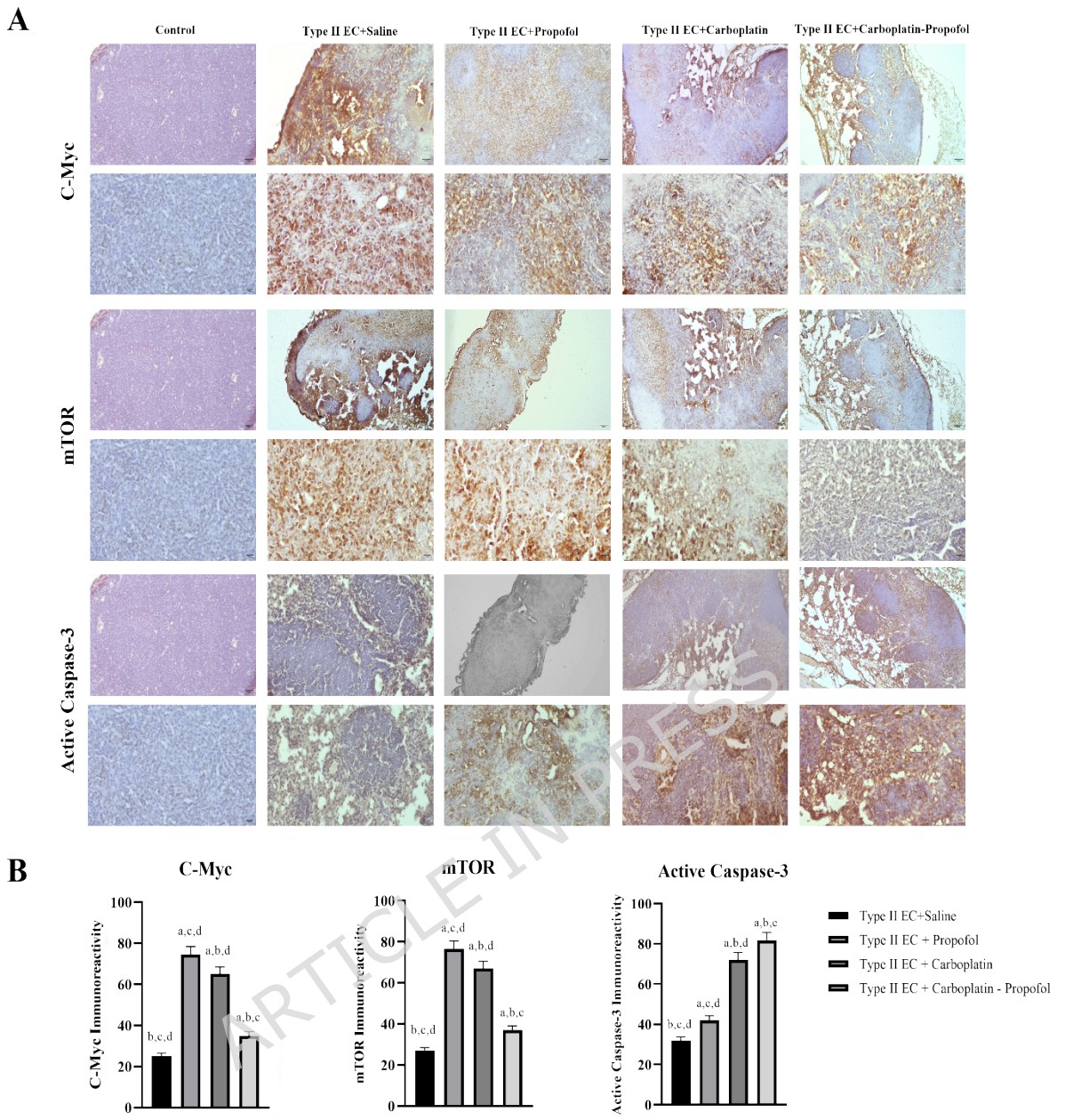

Figure 7. Immunohistochemical analysis of c-Myc, mTOR, Active Caspase-3 expression in Type II EC xenograft tumors following propofol and carboplatin treatment. Representative tumor sections illustrate decreased c-Myc and mTOR immunoreactivity in Propofol-, Carboplatin-, and combination-treated xenografts compared with untreated controls (Figure 7A). Low-magnification images are shown in the upper panels (scale bar: 100 µm), whereas high-magnification images are presented in the lower panels (scale bar: 20 µm). Semi-quantitative scoring demonstrates that combined Propofol–Carboplatin treatment resulted in the lowest expression levels of both markers among all groups (Figure 7B; $p<0.05$). *a*: significant change compared to saline group ($p<0.05$); *b*: significant change compared to propofol group ($p<0.05$); *c*: significant change compared to carboplatin group ($p<0.05$); *d*: significant change compared to propofol–carboplatin group ($p<0.05$). Data represent mean ± SD of n = 10 independent and non-overlapping fields. Statistical significance was determined using one-way ANOVA followed by Tukey's post-hoc test.

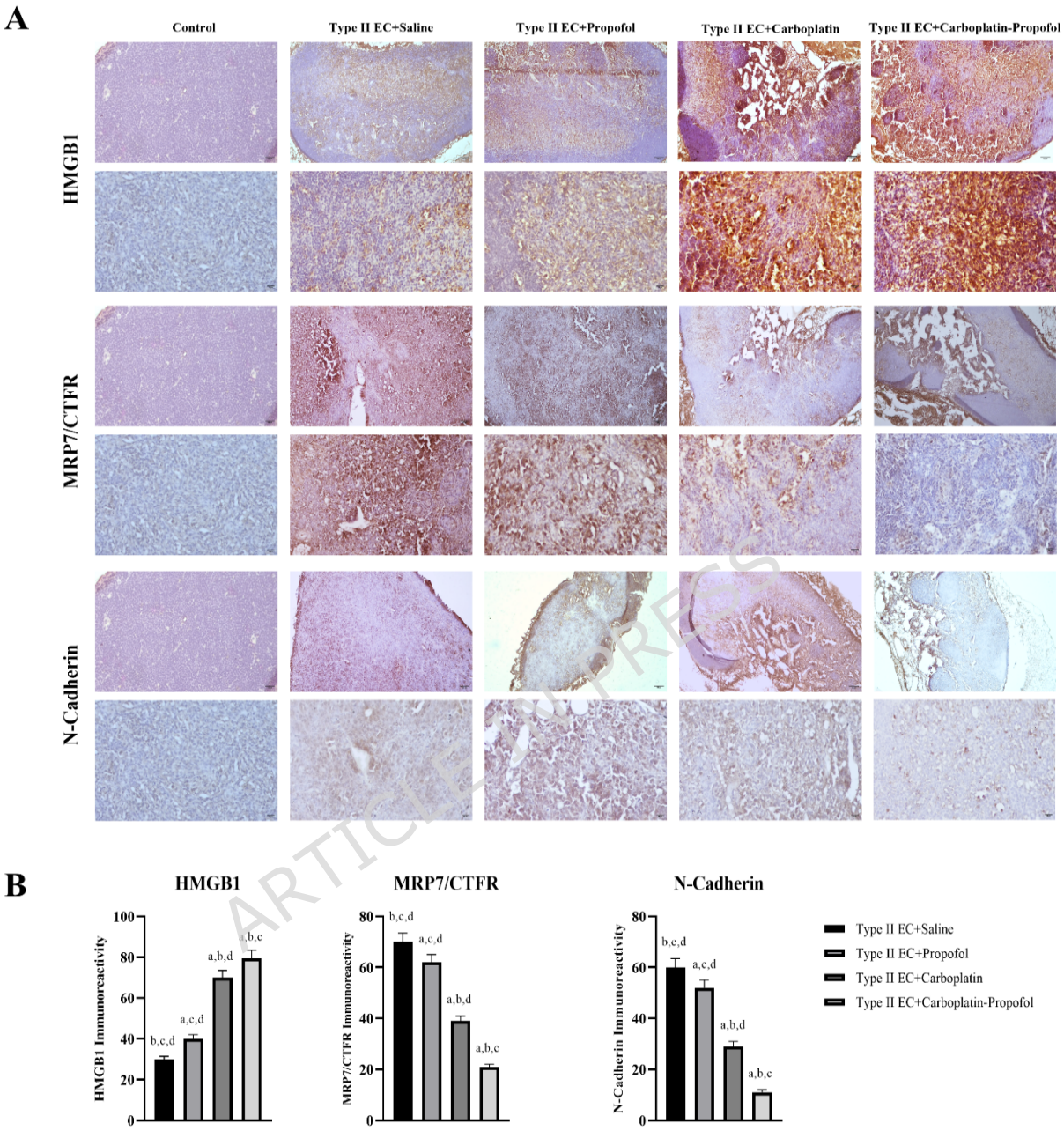

Figure 8. Immunohistochemical analysis of N-Cadherin and MRP7/CFTR expression in Type II EC xenograft tumors following propofol and carboplatin treatment. Representative tumor sections demonstrate reduced immunoreactivity of N-Cadherin and MRP7/CFTR in Propofol-, Carboplatin-, and combination-treated xenografts compared with untreated controls (Figure 8A). Low-magnification images are shown in the upper panels (scale bar: 100 μm), whereas high-magnification images are presented in the lower panels (scale bar: 20 μm). Semi-quantitative analysis indicates that combined Propofol–Carboplatin treatment resulted in the greatest reduction in the expression levels of both markers among all groups (Figure 8B; $p<0.05$). *a*: significant change compared to saline group ($p<0.05$); *b*: significant change compared to propofol group ($p<0.05$); *c*: significant change compared to carboplatin group ($p<0.05$); *d*: significant change compared to propofol–carboplatin group ($p<0.05$). Data represent mean ± SD of n = 10 independent and non-overlapping fields. Statistical significance was determined using one-way ANOVA followed by Tukey's post-hoc test.

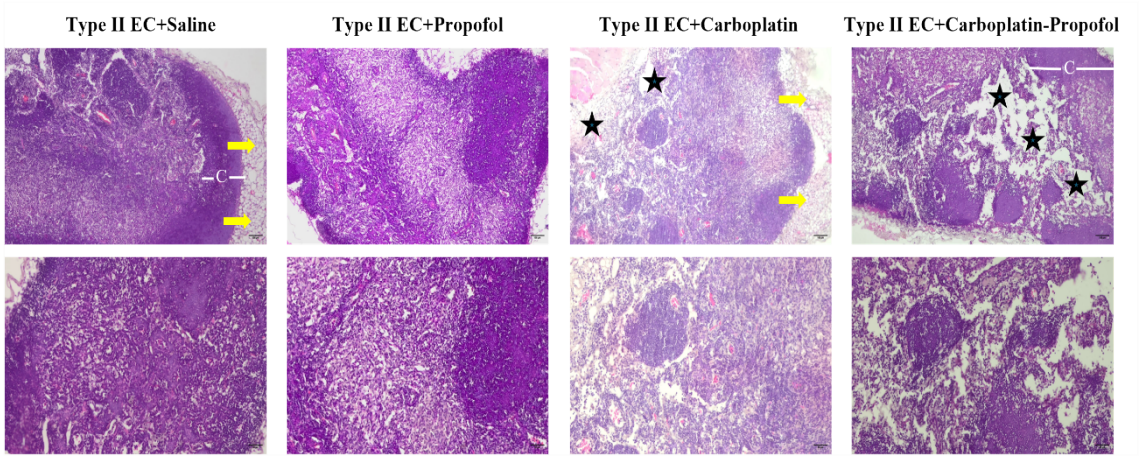

Figure 9. Histopathological features of Type II endometrial cancer xenograft tumors following propofol and carboplatin treatment. H&E-stained tumor sections reveal increased necrotic areas in all propofol-treated groups compared with untreated controls. Combination therapy with Propofol–Carboplatin is associated with more extensive tumor necrosis than carboplatin alone, accompanied by capsular thinning or disruption, reduced tumor-associated adipose tissue, increased immune cell infiltration, and diminished neoangiogenic regions. Low-magnification images are shown in the upper panels (scale bar: 100 µm), whereas high-magnification images highlighting necrotic and capsular regions are presented in the lower panels (scale bar: 20 µm). Comparative evaluation of propofol-treated and untreated tumors further demonstrates increased necrosis and capsular thinning, supporting a direct antitumoral effect of propofol. ***C*** indicate tumor capsule; ***yellow arrows*** indicate tumor-associated adipose tissue; ***asterisk*** indicates intratumoral necrosis.

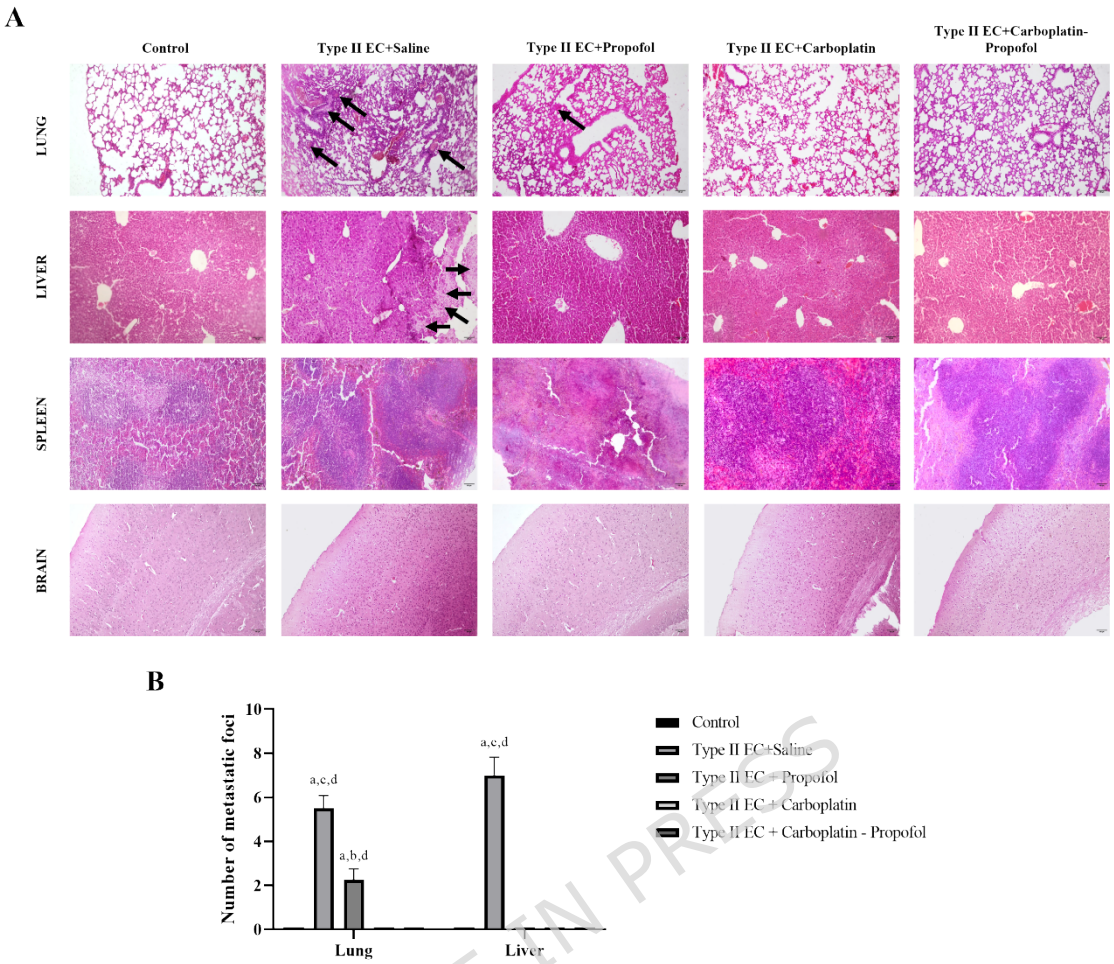

Figure 10. Histopathological assessment of distant organs in Type II endometrial cancer xenograft models following propofol and carboplatin treatment (Figure 10A). H&E-stained sections of lung and liver tissues demonstrate reduced metastatic involvement in propofol-treated groups compared with untreated controls (scale bar: 20 µm). Specimens from carboplatin-treated animals exhibited no detectable metastatic lesions but showed treatment-associated hemorrhage and edema, which were markedly attenuated by adjuvant propofol administration. No metastatic lesions were observed in brain or spleen tissues across experimental groups (Figure 10B). ***Black arrows*** indicate metastatic lesions. *a*: significant change compared to saline group ($p<0.05$); *b*: significant change compared to propofol group ($p<0.05$); *c*: significant change compared to carboplatin group ($p<0.05$); *d*: significant change compared to propofol–carboplatin group ($p<0.05$). Data represent mean ± SD of n = 10 independent and non-overlapping fields. Statistical significance was determined using one-way ANOVA followed by Tukey's post-hoc test.